# Core-halo mass relation in scalar field dark matter models and its consequences for the formation of supermassive black holes

Luis E. Padilla,[1,2,3,*] Tanja Rindler-Daller,[4,†] Paul R. Shapiro,[5,‡] Tonatiuh Matos,[1,§] and J. Alberto Vázquez[2,‖]

[1]*Departamento de Física, Centro de Investigación y de Estudios Avanzados del IPN,*
*A.P. 14-740, 07000 México D.F., México*
[2]*Instituto de Ciencias Físicas, Universidad Nacional Autónoma de México,*
*Apdo. Postal 48-3, 62251 Cuernavaca, Morelos, México*
[3]*Mesoamerican Centre for Theoretical Physics, Universidad Autónoma de Chiapas,*
*Carretera Zapata Km. 4, Real del Bosque (Terán), Tuxtla Gutiérrez 29040, Chiapas, México*
[4]*Institut für Astrophysik, Universitätssternwarte Wien,*
*University of Vienna, Türkenschanzstr. 17, 1180 Vienna, Austria*
[5]*Department of Astronomy and Texas Cosmology Center, The University of Texas at Austin,*
*2515 Speedway C1400, Austin, Texas 78712, USA*

Scalar-field dark matter (SFDM) halos exhibit a core-envelope structure with soliton-like cores and cold-dark matter(CDM)-like envelopes. Simulations without self-interaction (free-field case) have reported a core-halo mass relation of the form $M_c \propto M_h^\beta$, with either $\beta = 1/3$ or $\beta = 5/9$. These results can be understood if the core and halo follow some special energy or velocity scaling relations. We extend these core-halo mass relations here to include the case of SFDM with self-interaction, either repulsive or attractive, and investigate its implications for the possible gravitational instability and collapse of solitonic cores, leading to the formation of supermassive black holes (SMBHs). Core sizes are set by the larger of two length scales, the de Broglie wavelength (in the free-field limit) or the radius $R_{\rm TF}$ of the $(n = 1)$-polytrope for repulsive SFDM (in the Thomas-Fermi regime), depending upon particle mass $m$ and interaction strength $\lambda$. For parameters selected by previous literature to make approximately Kpc-sized cores and CDM-like structure formation on large scales but suppressed on small scales, we find that cores are stable for all galactic halos of interest, from the free-field to the repulsive Thomas-Fermi limit. For attractive self-interaction in this regime, however, halos of mass $M_h \sim 10^{10}$–$10^{12}$ $M_\odot$ have cores that collapse to form seed SMBHs with $M_{\rm SMBH} \sim 10^6$–$10^8$ $M_\odot$, as observations seem to require, while smaller-mass halos have stable cores, for particle masses $m = 2.14 \times 10^{-22}$–$9.9 \times 10^{-20}$ eV$/c^2$, if the free-field limit has $\beta = 1/3$, or $m = 2.23 \times 10^{-21}$–$1.7 \times 10^{-18}$ eV$/c^2$, if $\beta = 5/9$. We also place bounds on $\lambda$ for this case. For free-field and repulsive cases, if previous constraints on particle parameters are relaxed to allow much smaller (subgalactic scale) cores, then halos can also form SMBHs, for the same range of halo and black hole masses, as long as $\beta = 5/9$ is correct for the free-field limit. In that case, structure formation in SFDM would be largely indistinguishable from that in CDM. As such, while these SFDM models might not help to resolve the small-scale structure problems of CDM, they would explain the formation of SMBHs quite naturally, which is otherwise not a direct feature of CDM. Since CDM, itself, has not yet been ruled out, such SFDM models must also be viable.

## I. INTRODUCTION

Two of the greatest puzzles in contemporary cosmology and fundamental physics are:

1. The nature and origin of cosmic dark matter (DM).

2. The origin of the SMBHs observed in galactic nuclei.

Regarding the first point, the cosmological standard model ΛCDM suggests that DM is composed of a non-relativistic, collisionless gas—CDM—and usually assumed to be a weakly interacting massive particle (WIMP) which originated as a thermal relic of the big bang [1,2]. Although WIMP dark matter describes observations well at cosmological scales, it is in apparent conflict with some observations on small scales (e.g., the problem of cuspy-core-

[*]epadilla@fis.cinvestav.mx
[†]tanja.rindler-daller@univie.ac.at
[‡]shapiro@astro.as.utexas.edu
[§]tonatiuh.matos@cinvestav.mx
[‖]javazquez@icf.unam.mx

halo density profiles, overproduction of satellite dwarfs within the Local Group, and others; see, for example, Refs. [3–7]). In addition, all attempts to detect WIMPs directly in the laboratory or indirectly by astronomical signals from their decay or annihilation in distant objects [8] have been unsuccessful, and a large range of particle parameters originally predicted to be detectable have thereby been ruled out. For this reason, it seems necessary to explore alternative models to standard ΛCDM that help us to solve all these issues. With this in mind, several models have been proposed, one of which considers that the DM is composed of an ultralight real or complex scalar field, minimally coupled to gravity, and interacting only gravitationally with the rest of the matter as of a very early time in the cosmic evolution.

The main idea of scalar fields as the DM in the Universe originated about two decades ago [9–16], although some hints can be traced further back in Refs. [17,18]. Since then, the idea has been rediscovered by various authors with different names, for example, SFDM [14], fuzzy DM [11], wave DM [19], Bose-Einstein condensate DM [20], or ultralight axion DM [21] (see also Ref. [22]). However, its first systematic study started in Refs. [23,24]. In this work, we choose to call the model "SFDM."

In order for the scalar field to behave as a "cold" DM candidate, it is necessary that its Lagrangian possesses a quadratic term in the potential,

$$V(\varphi) = \frac{1}{2} \frac{m^2 c^2}{\hbar^2} \varphi^2, \qquad (1)$$

which gives rise to a pressureless fluid behavior in the matter-dominated epoch of the Universe, where SFDM dominates all other cosmic components.

The simplest models have only this term in the scalar field potential, i.e., there is one tunable parameter $m$, which is subject to constraints from observations, as we will describe below. Such models are usually termed "fuzzy dark matter"—we will often call it "free SFDM/free field" or "free case" in this paper. However, we are interested to study more varied models by considering the addition of a further term in the Lagrangian of the form

$$V(\varphi)_{\mathrm{SI}} = \frac{\lambda}{4\hbar c} \varphi^4. \qquad (2)$$

Similarly to the quadratic term, this quartic term may either stem directly from a fundamental particle description of SFDM, or it might result upon an expansion of a fundamental (even) potential, as, e.g., the cosine-type of "axion-like" particles. Self-interaction has been mostly neglected in previous literature, because of the smallness of the respective coupling parameter $\lambda$. However, it is only recently that the community has embarked on studying models with self-interaction in more detail, because it turns

out that self-interaction leads to qualitative differences, compared to the free case.

The astrophysical motivation to consider SFDM as a DM candidate has its root in the small-scale problems of CDM mentioned in the beginning. In order to reproduce galactic cores of order 1 kpc for the free SFDM case, the boson mass is typically assumed in the range of $m \sim 10^{-22}$–$10^{-20}$ eV/$c^2$. However, once self-interaction is included, the boson mass can be much higher than those values and yet produce large enough cores by tuning the ratio of $\lambda/m^4$. A reassessment of the different constraints in the literature, as well as including the implications of our work here, will be presented in a later section (for a review of SFDM, see Refs. [25–30]). Our work will focus on certain dynamical aspects of SFDM structure formation, namely the structure of equilibrium halos and possible implications for SMBH formation.

Simulations of SFDM cores without self-interaction [19,31–37] have shown that, upon multiple mergers, SFDM leads to cored density profiles in the inner region of galactic halos. These cores, referred to as "solitons" in the literature [19,35,38–40], have been shown to have a size of order of the de Broglie wavelength of individual bosons,

$$\lambda_{\mathrm{dB}} \propto \frac{1}{mv}, \qquad (3)$$

where $v$ is the "virial velocity" of the bosons, a result expected from analytic calculations. However, these cores have been found to be surrounded by a Navarro-Frenk-White-like envelope generated by quantum interference inherent to SFDM, following a relation of the form

$$M_c \propto M_h^\beta, \qquad (4)$$

where $M_c$ and $M_h$ are the total core and halo mass, respectively. The particular value of this $\beta$ parameter is still under debate, given that different authors have obtained different results. On the one hand, in Refs. [19,31], an expression that is well adjusted with a parameter $\beta = 1/3$ is found from their fully cosmological simulations. On the other hand, by adopting more simplified scenarios on galaxy formation but with better resolution, some authors [34,36] have found that a parameter $\beta = 5/9$ should describe correctly virialized core-halo mass structures in this scenario of SFDM. This correlation between the halo core and its "envelope" has not been anticipated by early work, though it is possible to understand the form of each correlation in an *a posteriori* way, using analytic arguments. Indeed, the fact that these correlations have been established by simulations, offers a unique opportunity to understand and extend the correlations by considering novel physical effects such as the addition of DM self-interaction.

The core-envelope structure of SFDM halos with self-interaction has not yet been established by three-dimensional cosmological simulations, and yet we expect such a structure, as well. Preliminary results of one-dimensional simulations show that a core-envelope structure also arises in the strongly self-interacting regime of SFDM, the so-called Thomas-Fermi (TF) regime (T.A.Dawoodbhoy, P.R.Shapiro, T.Rindler-Daller, to be subm.). This is good news for SFDM, because the (quantum) cores alone cannot explain the big range of galactic halo masses found in the Universe, and it is this simple observation which "mandates" that cores (with or without self-interaction) have to be enshrouded by some envelopes, if SFDM is regarded as an alternative to CDM. Early indications of the problem of the core-halo mass relationship and a toy model for the TF regime of SFDM can be found in Ref. [30]. Those authors suggested that the wave nature of SFDM would result in an effective pressure support (reflecting random wave motions and the associated density inhomogeneity implied on small scales) when averaged over scales larger than the core, leading to virial equilibrium on scales well beyond the size of the core, out to the same scales as in CDM halos, in fact. Halo envelopes were later confirmed in the fuzzy regime through simulations by Ref. [31] and follow-up studies, as referenced above.

In the first part of this work, we will extend the core-halo mass relation (4) to SFDM models with self-interaction, using analytical calculations. In all cases, the core mass increases with halo mass. Therefore, in the second part, we will apply our result to assess the SFDM parameter space for which soliton cores eventually become too massive to remain stable: beyond a critical mass, which depends upon SFDM parameters, soliton cores will collapse and can form black holes. This way, SFDM might provide a mechanism to form SMBHs in the centers of halos as of an early time. However, it turns out that it is very difficult to produce SMBHs with fiducial values of SFDM in the fuzzy regime, while SMBH formation is much more feasible, once self-interaction is added, as we will show.

There is a host of observations that indicate the existence of SMBHs—with masses ranging between $10^6$–$10^{10}$ $M_\odot$, placed in the center of most massive galaxies [41,42]. The origin of SMBHs is still mysterious, given their huge masses at the high redshifts ($z > 5.6$), where they have been observed [43–56]. In order for stellar black holes (BHs) to become supermassive, they would need to accrete large amounts of baryonic material and DM over a short time, which is unfeasible even if accretion happens at maximum Eddington rate. In addition to this puzzle of high-$z$ SMBHs, there is also a problem in understanding why there seem to be no medium-sized black holes with masses approximately $10^2$–$10^5$ $M_\odot$. Some standard scenarios of the formation of SMBHs consider the following: like stellar BHs, which result from the collapse of massive stars, SMBHs could be produced either by the collapse of massive clouds of gas during the early stages of formation of a galaxy [57] or by the collapse of supermassive Pop III stars.[1] Another suggestion considers the formation of a cluster of stellar BHs, which eventually merge into a SMBH [60]. However, it seems that these scenarios do not deliver a fully satisfactory explanation for the formation and evolution of such SMBHs at high redshifts. Additionally, observations show that the masses $M_{\mathrm{SMBH}}$ of the central SMBHs are correlated with various global properties of their host galaxies. The most important relationship concerns the mass of the SMBH and the bulge mass and an even tighter correlation with the stellar velocity dispersion of the host galaxy bulge, first reported by Refs. [61,62]. As a result, it has been also suggested that the central SMBH mass is correlated with the total mass of its host galaxy [63,64].

Observations might thus indicate that the formation and growth of SMBHs over time could be related to the DM-dominated galactic halos. With this in mind, Ref. [65] studies the possibility that SMBHs might form by collapse of all or part of gravitationally bound equilibrium objects made of SFDM, which are assumed to model nuclear galactic halos. Several earlier works have considered this scenario and studied its plausibility. Among them, it was demonstrated that self-gravitating objects comprising free scalar field configurations with masses larger than $0.6 \, m_{\mathrm{pl}}^2/m$, where $m_{\mathrm{pl}}$ is the Planck mass, are able to collapse and form a BH [66–72]. For the specific case of a mass $m \sim 10^{-22}$ eV/$c^2$, such configurations have a critical mass of collapse of approximately $10^{13}$ $M_\odot$. On the other hand, simulations in spherical symmetry demonstrated that only a part of the scalar field collapses to form a BH, while the remaining scalar field continues to surround the resulting BH for a very long time (longer than the age of the Universe) and can play the role of the DM halo of the galaxy [69,71,72]. It is important to mention that these studies conclude that most of the scalar field configuration collapses into a BH, leaving only a small scalar field remnant for the halo. However, these analyses have been performed in spherical symmetry and in a limited region of parameter space, corresponding to typical systems known as boson stars (BSs). Also, in these studies, those BSs have been used to model the entire SFDM halo, an unrealistic scenario, because simulations by Refs. [19,31–37] revealed that SFDM halos possess a more complicated core-envelope structure [see Eq. (4)]. However, the above results are nevertheless useful, given that such BSs represent very well the soliton profiles observed in the central region of a

---

[1]These scenarios are not to be confused with another (non-standard) proposal to explain SMBHs, namely so-called super-massive dark stars, primordial stars of supermassive size which are powered by DM self-annihilation in models of WIMP and related dark matter [58,59]. Once dark stars collapse, they could form seed black holes of about $10^4$–$10^5$ $M_\odot$.

galactic halo and then, given the fact that we are interested in an extension of the model to include self-interaction, simulations for the case of a self-interacting BS should be also applicable to the central soliton in halos. This case is of interest for the issue of studying the possible collapse of the central soliton within massive galactic halos (hosting massive galaxies). In fact, this last scenario is one of the main objectives of our study that will be analyzed in this work.

The paper is organized as follows. In Sec. II, we review the basic equations necessary to describe the self-interacting SFDM model: the Einstein-Klein-Gordon (EKG) system for a general description and the Gross-Pitaevskii-Poisson (GPP) system in the weak-field limit.[2] In Sec. III, we present a basic description of the SFDM soliton profile, which is obtained as the minimum-energy, coherent, quasistationary solution of the GPP. In the same section, we consider a Gaussian ansatz to describe the soliton in order to maintain some freedom in working with the self-interaction parameter of the SFDM model. We show that, in general, this ansatz maintains practically all the relations that are found in the numerical solution (e.g., the parameter dependence for the maximum mass for collapse of the soliton, parameter dependence in the TF regime, etc.), even those which result from a general-relativistic treatment. This implies that the Gaussian ansatz represents a good approximation for the soliton. Also in this section, we show that the results provided by this ansatz can be easily obtained in the hydrodynamic representation of the GPP system and by considering a simple dimensional argument, without the need of considering any functional form for the core profile. In Sec. IV, we extend the core-halo mass relation to self-interacting SFDM by assuming that some energy relations that are fulfilled by core and halo quantities in the simplest SFDM model remain valid in the self-interacting scenario. Because two relations have been reported between the masses of the core and the halo, we decided to extend both of them. In Sec. V, we compare our results with previous works, with the emphasis on the implied constraints of the SFDM model parameters. For this comparison, we focus on the core properties found in the central region of SFDM halos. We find that for a repulsive SFDM candidate, the central soliton remains stable and should be represented in the TF regime, while for attractive SFDM, we have scenarios where the soliton can collapse and form a SMBH within massive galactic halos (hosting massive galaxies), while the cores remain stable in those halos that host the least massive galaxies. Finally, in Sec. VI, we present our conclusions.

---

[2]In what follows, "weak field" refers to the regime of weak gravitational fields, i.e., the Newtonian regime.

## II. BASIC EQUATIONS FOR THE SCALAR FIELD DARK MATTER MODEL

In this section, we review the basic equations necessary to describe the dynamics of a scalar field minimally coupled to gravity. We consider a complex field, given that the case of a real field is easily derived from this description.

### A. Einstein-Klein-Gordon system

The set of differential equations governing the dynamics of a self-interacting scalar field minimally coupled to gravity is described by the EKG system,

$$\Box\varphi + 2\frac{dV(|\varphi|^2)}{d|\varphi|^2}\varphi = 0, \tag{5a}$$

$$R_{\alpha\beta} - \frac{1}{2}g_{\alpha\beta}R = \frac{8\pi G}{c^4}T_{\alpha\beta}, \tag{5b}$$

where

$$V(|\varphi|^2) = \frac{m^2c^2}{2\hbar^2}|\varphi|^2 + \frac{\lambda}{4\hbar c}|\varphi|^4, \tag{6}$$

$c$ is the speed of light, $\hbar$ is the reduced Planck constant, $G$ is the gravitational constant, $\lambda$ is a self-interaction parameter that can be positive (repulsive) or negative (attractive), $\Box \equiv \nabla_\mu\nabla^\mu$ is the 4-D'Alembert operator, $\varphi$ is the scalar field with units $[\sqrt{kg \cdot m}/s]$, $g_{\alpha\beta}$ is the spacetime metric, $R_{\alpha\beta}(R)$ is the Ricci tensor (scalar), and $T_{\alpha\beta}$ is the stress energy tensor which possesses all the energy components that exist in the system. Particularly, for the scalar field,

$$T_{\alpha\beta}^{(\varphi)} = \frac{1}{2}(\nabla_\alpha\varphi)^*(\nabla_\beta\varphi) + \frac{1}{2}(\nabla_\alpha\varphi)(\nabla_\beta\varphi)^*$$
$$- g_{\alpha\beta}\left[\frac{1}{2}(\nabla^\gamma\varphi)^*(\nabla_\gamma\varphi) - V(|\varphi|^2)\right]. \tag{7}$$

Here, greek letters range from 0 to 3, denoting spacetime indices.

### B. Weak-field limit

Structure formation of halos in a matter-dominated Universe can be well described within the weak-field limit. In this limit, Eq. (5) is reduced to the GPP system [73]

$$i\hbar\frac{\partial\psi}{\partial t} = -\frac{\hbar^2}{2m}\nabla^2\psi + m\Phi\psi + g|\psi|^2\psi, \tag{8a}$$

$$\nabla^2\Phi = 4\pi G\rho, \tag{8b}$$

where $\psi$ is defined in terms of $\varphi$ as

$$\varphi(\mathbf{x}, t) = \frac{\hbar}{\sqrt{m}} e^{-imc^2 t/\hbar} \psi(\mathbf{x}, t), \qquad (9)$$

$g \equiv \lambda\hbar^3/(2m^2 c)$, $\Phi$ is the gravitational potential, and $\rho$ is a cosmological overdensity that usually possesses contributions from the DM and the baryonic components. If we ignore the baryonic contribution (a limitation shared with most of the simulation work [19,31–35]), we have $\rho = m|\psi|^2$.

Observe that by using in (6) the new field $\psi$ defined in (9) and the definition of $g$, we obtain

$$V(|\psi|^2) = \frac{mc^2}{2}|\psi|^2 + \frac{g}{2}|\psi|^4, \qquad (10)$$

which is the scalar field potential in standard physical units.

Two important quantities that are necessary to describe SFDM halos are the total mass $M_t$ and total energy $E_t$ associated with the system:

$$M_t = m \int_V |\psi|^2 d^3\mathbf{r}, \qquad (11a)$$

$$E_t = \int_V \left[ \frac{\hbar^2}{2m}|\nabla\psi|^2 + \frac{m}{2}\Phi|\psi|^2 + \frac{g}{2}|\psi|^4 \right] d^3\mathbf{r}. \qquad (11b)$$

Observe that the total energy can be written in a very instructive way,

$$E_t = K_t + W_t + U_{\mathrm{SI},t}, \qquad (12)$$

where

$$K_t = \int_V \frac{\hbar^2}{2m}|\nabla\psi|^2 d^3\mathbf{r} \qquad (13a)$$

is the total kinetic energy,

$$W_t = \int_V \frac{m}{2}\Phi|\psi|^2 d^3\mathbf{r} \qquad (13b)$$

is the total gravitational potential energy, and

$$U_{\mathrm{SI},t} = \int_V \frac{g}{2}|\psi|^4 d^3\mathbf{r} \qquad (13c)$$

is the total energy associated with the self-interaction. This last way of writing each energy contribution is very convenient, because they also appear in the scalar virial theorem of an isolated mass distribution,

$$2K_t + W_t + 3U_{\mathrm{SI},t} = 0. \qquad (14)$$

On the other hand, notice that if we use the variables

$$\hat{\psi} = \sqrt{\frac{4\pi G\hbar^2}{mc^4}}\psi, \qquad \hat{\mathbf{r}} = \frac{mc}{\hbar}\mathbf{r}, \qquad \hat{t} = \frac{mc^2}{\hbar}t,$$

$$\hat{\Phi} = \frac{\Phi}{c^2}, \qquad \hat{\Lambda} = \frac{c^2 g}{4\pi G\hbar^2} = \frac{m_{\mathrm{pl}}^2}{m^2}\frac{\lambda}{8\pi} \qquad (15)$$

(note that $mc/\hbar$ is the inverse Compton length and $mc^2/\hbar$ is the bare angular frequency of the field), the GPP system can be rewritten in a way where all the natural constants disappear:

$$i\frac{\partial\hat{\psi}}{\partial\hat{t}} = -\frac{1}{2}\hat{\nabla}^2\hat{\psi} + \hat{\Phi}\,\hat{\psi} + \hat{\Lambda}|\hat{\psi}|^2\hat{\psi}, \qquad (16a)$$

$$\hat{\nabla}^2\hat{\Phi} = |\hat{\psi}|^2. \qquad (16b)$$

Additionally, there is a rescaling property for this GPP system given by

$$\{\hat{t}, \hat{\mathbf{r}}, \hat{\Lambda}, \hat{\psi}, \hat{\Phi}\} \Rightarrow \{\gamma^2\hat{t}, \gamma\hat{\mathbf{r}}, \gamma^2\hat{\Lambda}, \gamma^{-2}\hat{\psi}, \gamma^{-2}\hat{\Phi}\}, \qquad (17)$$

where $\gamma > 0$ is a scaling parameter. Then, the different physical quantities defined in (11) and (13) are also rescaled with similar relations.

## III. SOLITON PROPERTIES: GENERAL CONSIDERATIONS

### A. Weak-field limit

It has been accepted that, for the long timescales of structure formation, the averaged density profile of cores appearing in central regions of SFDM halos can be well fit by coherent, quasistationary, ground-state solutions of the GPP system. In this section, we review different previous results which we will use in order to extend the soliton description to self-interacting SFDM particles.

Quasistationary states of (16) are described by dimensionless wave functions of the form

$$\hat{\psi}(\hat{\mathbf{r}}, \hat{t}) = \hat{\phi}(\hat{r})e^{-i\hat{\mu}\hat{t}}, \qquad \hat{\mu}, \hat{\phi} \in \mathbb{R}, \qquad (18)$$

where $\hat{r}$ is the dimensionless spherical radial coordinate and $\hat{\mu}$, the dimensionless GPP chemical potential, should be fixed by the conservation of particle number. In general, the system (16) with the ansatz (18) has an infinite number of different solutions that fulfill appropriate initial and boundary conditions [74,75].[3] Each of them—usually called Newtonian boson stars (NBSs)—can be identified by the number of nodes (= zeros) of $\hat{\phi}$, before the solution decays asymptotically. The solution without nodes—the soliton— is considered the ground state of the GPP system, and it

---

[3]The typical boundary conditions are given by regularity in the origin $\hat{\phi}(\hat{r} = 0) = \hat{\phi}_0$, $\hat{\phi}'(\hat{r} = 0) = 0$ and asymptotic vanishing $\hat{\phi}(\hat{r} \to \infty) \to 0$, $\hat{\Phi}(\hat{r} \to \infty) \simeq -M/r^2$.

possesses the smallest value of $\hat{\mu}$, while solutions with nodes are usually excited NBSs.

Observe that from (17), it is possible to construct different solutions for the soliton, once one of them is known. In fact, as explained in Ref. [75], in the free case, it is possible to construct all the ground-state solutions for a given central scalar field value, just by using the rescaling property in (17). On the other hand, in the self-interacting case, something similar occurs: once a ground-state solution is known for a given value of $\hat{\Lambda}$, it is possible to construct all the ground-state solutions for different central value of the scalar field and the same value of $\hat{\Lambda}$, just by using the rescaling properties provided in (17). However, if we were interested in finding a new soliton with a different $\hat{\Lambda}$, it would be necessary to solve the differential equations (16) for such $\hat{\Lambda}$ again. Therefore, we can see that once a self-interaction parameter is added to the model, we do not have the same freedom in working with the soliton solution, as in the free case. Nevertheless, as we shall see in this section, we can avoid this problem, once a Gaussian approximation is adopted. In addition, we will also show that the results obtained from the Gaussian ansatz can be reconstructed by considering a dimensional argument. To this end, let us continue to present some basic relations that will be helpful for our later description and apply them to the case of the free field in order to compare with our Gaussian ansatz later.

First of all, all soliton solutions are virialized structures that fulfill Eq. (14).

Now, let us focus on the free case. Usually one solves for that solution for which the central value $\hat{\psi}(\hat{r} = 0) = 1$. In this case, the numerical value of the dimensionless chemical potential is $\hat{\mu} \simeq -0.69$. Such a solution can be used, together with the rescaling parameter $\gamma$ in (17), to construct solitons with different masses by fixing the $\gamma$ parameter as [76]

$$\gamma = 3.6 \times 10^{-6} m_{22} M_{c,7}^{(\gamma)}, \qquad (19)$$

where $M_{c,7}^{(\gamma)} \equiv M_c^{(\gamma)}/(10^7\ M_\odot)$ and

$$m_{22} \equiv m/(10^{-22}\ \text{eV}/c^2).$$

Notice that we have left explicitly the $\gamma$ dependence for the numerical solution of the soliton.

Another important quantity is the radius that contains 99% of the soliton mass,

$$R_{99}^{(\gamma)} = 9.9 \frac{\hbar^2}{G M_c^{(\gamma)} m^2}, \qquad (20)$$

(see, for example, Ref. [22]), or in fiducial notation

$$R_{99}^{(\gamma)} \simeq \frac{8.445 \times 10^4}{(m_{22})^2 M_{c,7}^{(\gamma)}}\ \text{pc}. \qquad (21)$$

Finally, the soliton fulfils the relations

$$M_c^{(\gamma)} \simeq 4.3 \sqrt{\frac{|E_c^{(\gamma)}|}{M_c^{(\gamma)}}} \frac{m_{\text{pl}}^2}{mc}, \qquad (22\text{a})$$

$$M_c^{(\gamma)} \simeq 2.6 \left( \frac{|E_c^{(\gamma)}|}{(mG/\hbar)^2} \right)^{1/3}, \qquad (22\text{b})$$

which was found in Ref. [76]. In the free case, these relations are equivalent to

$$M_c^{(\gamma)} \simeq 4.3 \sqrt{\frac{K_c^{(\gamma)}}{M_c^{(\gamma)}}} \frac{m_{\text{pl}}^2}{mc} = 4.3 \sqrt{\frac{|W_c^{(\gamma)}|}{2 M_c^{(\gamma)}}} \frac{m_{\text{pl}}^2}{mc}, \qquad (23\text{a})$$

$$M_c^{(\gamma)} \simeq 2.6 \left( \frac{K_c^{(\gamma)}}{(mG/\hbar)^2} \right)^{1/3} = 2.6 \left( \frac{|W_c^{(\gamma)}|}{2(mG/\hbar)^2} \right)^{1/3}, \qquad (23\text{b})$$

which has been pointed out in Ref. [77].

*Remark 1.* We note that, thanks to the rescaling property of GPP, the configuration does not *per se* admit an upper critical mass. However, from general-relativistic calculations follow a limiting maximum mass beyond which collapse to a BH occurs. Only for attractive self-interactions, $\hat{\Lambda} < 0$, there is a maximum mass, even within the Newtonian description, given by [78,79],

$$M_{c,\text{max}} \simeq 10.03 \frac{m_{\text{pl}}}{\sqrt{|\lambda|}}, \qquad (24)$$

where we have decided to use $\lambda$ instead of $\hat{\Lambda}$ for simplicity in the expression; the $\hat{\Lambda}$ dependence for the above critical mass can be easily obtained from (15).

### 1. Gaussian ansatz in the weak-field limit

Previous literature has made extensive use of two different analytic approximations for the numerically evaluated ("exact") soliton profile of SFDM halos without self-interaction. On the one hand, there is a rational function approximation, which was proposed in Ref. [19], and which is based upon an "empirical fit" to the central region of halos from simulations (call it the Schive profile). On the other hand, a Gaussian profile has been used to approximate SFDM solitons in Refs. [38,80]. The use of a Gaussian distribution is motivated by the fact that Gaussian "wave packets" not only appear in many contexts of a linear Schrödinger equation, it also constitutes a solution for laboratory Bose-Einstein condensates without particle self-interaction; see, e.g., Ref. [81]. In this work, we decided to use the Gaussian profile, given its better physical foundation and the fact that it is easier to find physical relations of interest from it, given the difficulties described above with respect to the quasistationary states of variable $\hat{\Lambda}$. The difference between the two analytic profiles can be seen in

Appendix: the Schive profile appears to match better the numerical result for the soliton if $\hat{r}$ is small, while the Gaussian matches better the numerical solution at large $\hat{r}$. However, what is more important in our context is the fact that the Gaussian ansatz arrives at the same physical relationships than the numerical solution, and only the numerical prefactors differ by order 1 factors.

Now, the question arises as to what extent the Gaussian can be used, if self-interaction is included. In fact, Ref. [81] already used a Gaussian ansatz as a trial function in a variational analysis, in order to find modified physical relationships, valid when self-interaction is included. The same approach is proposed in Ref. [38] in order to extend the modeling of the SFDM soliton profile with self-interaction by considering the Gaussian density distribution

$$\rho_c^{(g)}(r) = \frac{M_c}{(\pi R_c^2)^{3/2}} e^{-r^2/R_c^2}, \tag{25}$$

where $R_c$ is a characteristic core radius associated with the radius that contains 99% of the total mass of the distribution[4] as $R_{99} = 2.38167 R_c$. For the sake of the reader, let us quote some of the results which follow from this approach: a mass-radius relation is found in Ref. [38] by way of minimizing the energy functional (11b) or (12) and considering the ansatz (25) as a trial function. That procedure yields

$$M_c = 3\sqrt{2\pi} \frac{\frac{\hbar^2}{Gm^2 R_c}}{1 - \frac{6g}{4\pi Gm^2 R_c^2}} \tag{26}$$

or, equivalently,

$$M_{c,7} \simeq \frac{10.076 \times 10^5}{m_{22}} \frac{\hat{R}_c}{\hat{R}_c^2 - 6\hat{\Lambda}}, \tag{27}$$

which is plotted in Fig. 1. As we already mentioned, $\hat{R}_c$ and $\hat{\Lambda}$ can be calculated from Eq. (15). We can solve this equation for the radius, in turn,

$$R_c = \frac{3\sqrt{2\pi}\hbar^2}{2Gm^2 M_c} + \sqrt{\left(\frac{3\sqrt{2\pi}\hbar^2}{2Gm^2 M_c}\right)^2 + \left(\frac{6g}{4\pi Gm^2}\right)^2}, \tag{28}$$

or in fiducial notation:

$$\hat{R}_c = \frac{5.04 \times 10^5}{M_{c,7}m_{22}} \left[1 + \sqrt{1 + 6\hat{\Lambda}\left(\frac{M_{c,7}m_{22}}{5.04 \times 10^5}\right)^2}\right]. \tag{29}$$

For $\hat{\Lambda} = 0$, we recover the mass-radius relationship in the free case. On the other hand, when $\hat{\Lambda} > 0$ and if the

---

[4]This number follows simply by calculating the radius which includes 99%, i.e., $2\sigma$ of the mass of the Gaussian distribution.
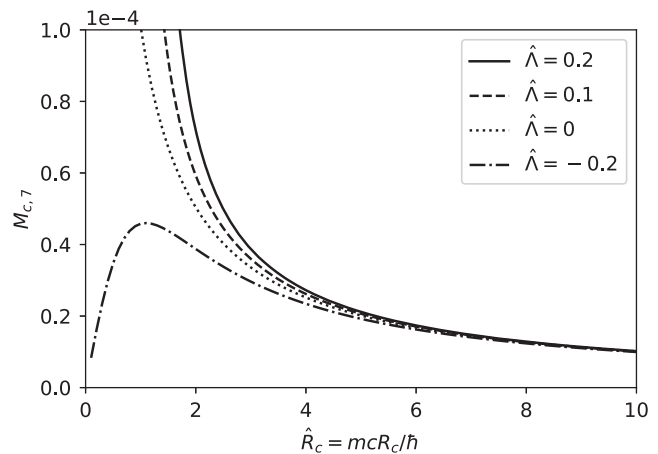


FIG. 1. Mass-radius relation of the soliton in self-interacting SFDM models: we plot Eq. (27) for $m_{22} = 1$ and various self-interaction strengths $\hat{\Lambda}$. The particular values of $\hat{\Lambda}$ were chosen in such a way that they coincide with those reported in Ref. [75] in order to simplify the comparison with their numerical result.

second term in the square root dominates, we obtain $\hat{R}_c \simeq \hat{R}_c^{(\mathrm{TF})} \equiv \sqrt{6\hat{\Lambda}}$, independent of $M_{c,7}$. In physical units, the radius in this regime of strong self-interaction reads $R_c \simeq \sqrt{6g/(4\pi Gm^2)}$, which recovers the form of the so-called Thomas-Fermi radius

$$R^{(\mathrm{TF})} = \pi\sqrt{\frac{g}{4\pi Gm^2}}, \tag{30}$$

which corresponds to the radius of an $(n = 1)$-polytrope (see Refs. [82,83]).[5]

By comparing Fig. 1 and the numerical solution (Fig. 1 in Ref. [75]), we can see that the relation (26) or (27) maintains the same basic parameter dependence than the numerical solution. For the attractive case ($\hat{\Lambda} < 0$), this means that there exists a maximum mass (upper bound mass) allowed by the scalar field configuration given by

$$M_{c,\mathrm{max}} \simeq 7.70 \frac{m_{\mathrm{pl}}}{\sqrt{|\lambda|}}, \tag{31}$$

[see also Eq. (24)], while in the repulsive and free case ($\hat{\Lambda} \geq 0$), there is no upper bound for the soliton mass. These statements all apply in the weak-field (Newtonian) limit. Another important property that is also maintained is the fact that the larger the coefficient $\hat{\Lambda}$, the more massive the equilibrium configuration. Interestingly, the radius at which the attractive case reaches its maximum mass is given by

---

[5]We can compare the radius that contains 99% of the total mass of the Gaussian ansatz and the radius obtained in the TF regime: considering that for the Gaussian ansatz $R_{99} \simeq 2.38167 R_c^{(\mathrm{TF})} \simeq 5.834\sqrt{g/(4\pi Gm^2)}$, we can see that both quantities are close within a factor of 2–3.

$\hat{R}_c = \hat{R}_{c,\mathrm{min}} \equiv \sqrt{6|\hat{\Lambda}|}$, which[6] is just the same radius at which the repulsive case goes over to the TF regime.

Now, we can easily show that the different energies defined in (12) and (13) are as follows for the SFDM Gaussian ansatz with self-interaction,

$$E_c = -\left[\frac{3\hbar^2 M_c}{4m^2 R_c^2} + \frac{gM_c}{2\sqrt{2}\pi^{3/2}m^2 R_c^3}\right], \qquad (32\mathrm{a})$$

$$K_c = \frac{3}{4}\frac{\hbar^2 M_c}{m^2 R_c^2}, \qquad (32\mathrm{b})$$

$$W_c = -\frac{GM_c^2}{2\sqrt{2\pi}R_c}, \qquad (32\mathrm{c})$$

$$U_{\mathrm{SI},c} = \frac{gM_c}{4\pi\sqrt{2\pi}m^2 R_c^3}, \qquad (32\mathrm{d})$$

where in the expression for $E_c$ we have used the virial theorem (14), applied to the core. Equation (32b) can be rearranged to

$$\frac{1}{R_c} = \frac{2m}{\sqrt{3}\hbar}\left(\frac{K_c}{M_c}\right)^{1/2}. \qquad (33)$$

Using the $M_c - R_c$ relation [see Eq. (26)], we arrive at

$$M_c \simeq 8.68\frac{m_{\mathrm{pl}}^2}{m}\frac{(\frac{K_c}{M_c})^{1/2}/c}{1 - 8\hat{\Lambda}(\frac{K_c}{M_c})/c^2}. \qquad (34)$$

Observe that in the free case ($\hat{\Lambda} = 0$), the above result differs from the result of simulations in Eq. (23a) only by a factor of 2. In a similar way, by interchanging $K_c \to -E_c$ (by using the virial theorem in the free-field limit), the above expression differs from (22a) by a factor of 2 as well.

We can reexpress the energies in (32) per core mass (i.e., specific energies), using the mass-radius relation (26) as

$$\frac{E_c}{M_c} = -\frac{1}{4\sqrt{2\pi}}\left(\frac{GM_c}{R_c}\right)\left[1 \pm \frac{1}{3}\left(\frac{R_{\mathrm{crit}}}{R_c}\right)^2\right], \qquad (35\mathrm{a})$$

$$\frac{K_c}{M_c} = \frac{1}{4\sqrt{2\pi}}\left(\frac{GM_c}{R_c}\right)\left[1 \mp \left(\frac{R_{\mathrm{crit}}}{R_c}\right)^2\right], \qquad (35\mathrm{b})$$

$$\frac{W_c}{M_c} = -\frac{1}{4\sqrt{2\pi}}\left(\frac{GM_c}{R_c}\right)\left[2 \mp \frac{3}{2}\left(\frac{R_{\mathrm{crit}}}{R_c}\right)^2\right], \qquad (35\mathrm{c})$$

$$\frac{U_{\mathrm{SI},c}}{M_c} = \frac{1}{4\sqrt{2\pi}}\left(\frac{GM_c}{R_c}\right)\left[\pm\frac{1}{6}\left(\frac{R_{\mathrm{crit}}}{R_c}\right)^2\right], \qquad (35\mathrm{d})$$

where the upper (lower) sign is for a repulsive (attractive) self-interaction, and in the above expressions, we have defined $R_{\mathrm{crit}} \equiv \sqrt{6|g|/(4\pi Gm^2)}$, in such a way that when $g > 0$, $R_{\mathrm{crit}} = R_c^{(\mathrm{TF})}$, whereas when $g < 0$, $R_{\mathrm{crit}} = R_{c,\mathrm{min}}$.

Finally, observe that in the free case, we obtain from (29), expressed in fiducial units

$$R_c \simeq \frac{6.44 \times 10^4}{(m_{22})^2 M_{c,7}} \ \mathrm{pc}. \qquad (36)$$

The radius $R_{99}$ that contains 99% of the total mass of the soliton is $R_{99} = 2.38167 R_c$, which from the above equation yields

$$R_{99} \simeq \frac{15.34 \times 10^4}{(m_{22})^2 M_{c,7}} \ \mathrm{pc}, \qquad (37)$$

as compared to the numerical result in (21).

Additionally, if we use equations (35a), (35b), and (35c) together with our mass-radius relation (26), we can express the core mass in the free-field limit as

$$M_c \simeq 4.22\left(\frac{|E_c|}{(mG/\hbar)^2}\right)^{1/3}, \qquad (38\mathrm{a})$$

$$M_c \simeq 4.22\left(\frac{K_c}{(mG/\hbar)^2}\right)^{1/3}, \qquad (38\mathrm{b})$$

$$M_c \simeq 4.22\left(\frac{|W_c|}{2(mG/\hbar)^2}\right)^{1/3}. \qquad (38\mathrm{c})$$

Comparing (37) with the numerical result in (21), or (38) with (22b) and (23b), we see that the difference between the results from the Gaussian ansatz versus the exact numerical solution is small, of a factor of a few.

### 2. Understanding the mass-radius relation for the solitonic core from the hydrodynamic representation of the GPP system

While the Gaussian ansatz has been extensively used in the literature and is well motivated to represent the numerical ground-state solution of the GPP system, we include yet another derivation of the mass-radius relation in this subsection, independent of the choice of functional form of the "trial function." For that purpose, we use the hydrodynamic representation of the GPP system.

By decomposing the wave function $\psi$ in polar form as

$$\psi(\mathbf{r}, t) = \sqrt{\frac{\rho(\mathbf{r}, t)}{m}}e^{iS(\mathbf{r}, t)} \qquad (39)$$

---

[6]Notice that in referring to this radius we use the subscript "min." The reason we use this subscript is because, as we will see later, this critical mass also corresponds to the minimum radius at which these configurations remain stable (see also Ref. [38]).

and defining a velocity field as

$$\bar{v} = \frac{\hbar}{m} \nabla S, \tag{40}$$

the GPP system is rewritten as an Euler and a continuity equation given by

$$\rho \frac{\partial \bar{v}}{\partial t} + \rho(\bar{v} \cdot \nabla)\bar{v} = -\rho \nabla Q - \rho \nabla \Phi - \nabla P_{\text{SI}}, \tag{41a}$$

$$\frac{\partial \rho}{\partial t} + \nabla \cdot (\rho \bar{v}) = 0, \tag{41b}$$

where

$$Q \equiv -\frac{\hbar^2}{2m^2} \frac{\nabla^2 \sqrt{\rho}}{\sqrt{\rho}} \quad \text{and} \quad P_{\text{SI}} \equiv \frac{g}{2m^2} \rho^2. \tag{42}$$

The term $Q$ is known as the quantum potential which arises from the quantum nature of SFDM, while $P_{\text{SI}}$ can be interpreted as a pressure term that is generated by the self-interaction between SFDM particles. In order to understand the parameter dependence of the soliton profile in the self-interacting SFDM model, we consider the following simplification: soliton structures fulfil $\partial \bar{v}/\partial t = 0 = \bar{v}$. Also, for simplicity we set $\nabla \sim 1/\mathcal{R}_c$, where $\mathcal{R}_c$ is the characteristic radius of the system; then,

$$\nabla Q \sim -\frac{\hbar^2}{2m^2 \mathcal{R}_c^3}, \qquad \nabla P_{\text{SI}} \sim -\frac{g\rho^2}{2m^2 \mathcal{R}_c},$$

$$\nabla \Phi \sim \frac{GM_c}{\mathcal{R}_c^2}, \tag{43}$$

where we choose the sign in $\nabla P_{\text{SI}}$ in such a way that this term correctly describes an attractive/repulsive pressure term, which is also consistent with the Gaussian ansatz. Using $\rho \sim 3M_c/(4\pi \mathcal{R}_c^3)$, which is equivalent to saying that the soliton profile possesses a nearly constant density, we obtain from (41)

$$-\frac{\hbar^2}{2m^2 \mathcal{R}_c^2} + a\frac{GM_c}{\mathcal{R}_c} - b\frac{3gM_c}{8\pi m^2 \mathcal{R}_c^3} = 0, \tag{44a}$$

$$\frac{\partial \rho}{\partial t} = 0, \tag{44b}$$

where $a$ and $b$ are some constants that we introduced to apply the summation in the above expression (i.e., we are considering, for example, that $\nabla Q \simeq \text{const} * \hbar^2/(2m^2 \mathcal{R}_c^3)$, and then, these constant parameters can be seen as small corrections that correctly relate the derivative to the characteristic radius $\mathcal{R}_c$).

First, Eq. (44b) reflects our assumption of a stationary solution, which is in agreement with (18). On the other hand, from (44a) and considering that $g > 0$, we obtain

$$a\frac{GM_c}{\mathcal{R}_c} = \frac{\hbar^2}{2m^2 \mathcal{R}_c^2} + b\frac{3gM_c}{8\pi m^2 \mathcal{R}_c^3}, \tag{45}$$

and so it is easy to see that solitons are produced by the equilibrium between self-gravity (left-hand side in the above expression) and the pressures due to quantum uncertainty and self-interaction.

Two well-studied limit cases are:

(i) *The fuzzy limit.*—This regime is obtained when the second term on the right-hand side of Eq. (45) can be ignored, and then the soliton is a result of the equilibrium between quantum pressure and gravity. In this limit, the $M_c - \mathcal{R}_c$ relation reads

$$M_c \mathcal{R}_c = \frac{1}{2a} \frac{\hbar^2}{Gm^2}, \tag{46}$$

which maintains the same parameter dependence found in the numerical treatment; see Eq. (20).

(ii) *The Thomas-Fermi approximation.*—This regime is obtained when the first term on the right-hand side of Eq. (45) can be ignored, and then the soliton results an equilibrium between gravity and the pressure due to self-interaction. In this limit, the soliton fulfills the $M_c - \mathcal{R}_c$ relation

$$\mathcal{R}_c = \sqrt{\frac{b}{2a} \frac{3g}{4\pi Gm^2}}, \tag{47}$$

which also maintains the same parameter dependence found by the exact solution; see Eq. (30).

On the other hand, if $g < 0$, we have

$$a\frac{GM_c}{\mathcal{R}_c} + b\frac{3|g|M_c}{8\pi m^2 \mathcal{R}_c^3} = \frac{\hbar^2}{2m^2 \mathcal{R}_c^2}, \tag{48}$$

and then the soliton results as an equilibrium between gravity plus self-interaction pressure and the repulsion due to the quantum pressure. Observe that in this scenario, we can also define a new limiting case

(i) *The strong self-interaction regime in the attractive scenario.*—This regime is obtained when the first term on the left-hand side of Eq. (48) can be ignored, and then the soliton can be understood as the equilibrium between quantum pressure and attractive self-interaction. In this limit, the $M_c - \mathcal{R}_c$ relation is

$$\mathcal{R}_c = b\frac{3|g|}{4\pi \hbar^2} M_c. \tag{49}$$

These configurations correspond to soliton profiles with radius smaller than the one with the maximum possible mass shown in Fig. 1. However, as already

mentioned in footnote 7, these configurations turn out to be unstable.

Rearranging Eq. (44a), we have

$$M_c = \frac{1}{2a} \frac{\frac{\hbar^2}{Gm^2 \mathcal{R}_c}}{1 - \frac{b}{2a} \frac{3g}{4\pi Gm^2 \mathcal{R}_c^2}}, \quad (50)$$

and it is easy to see that this relation is equivalent to the one shown in (26) from the Gaussian ansatz.

At this point, we have not yet specified the numerical values of $a$ and $b$. In order to do so, we could proceed in two different ways. First, we use the result from the Gaussian ansatz and set $\mathcal{R}_c = R_c$. In this case,

$$\frac{1}{2a} = 3\sqrt{2\pi}, \qquad \frac{b}{2a} = 2, \quad (51)$$

and the $M_c - R_c$ relation is then given exactly by (26). On the other hand, we could also fix the numerical values of $a$ and $b$ by matching our result with the exact numerical solution. For example, let us suppose that $R$ is the radius that contains 99% of the total mass of the configuration and that such a radius can always be written as $R = \text{const} * \mathcal{R}_c$. Then, from (50), we obtain

$$M_c = \frac{1}{2\hat{a}} \frac{\frac{\hbar^2}{Gm^2 R}}{1 - \frac{\hat{b}}{2\hat{a}} \frac{3g}{4\pi Gm^2 R^2}}, \quad (52)$$

where $\hat{a}$ and $\hat{b}$ are new constants. By matching the last expression with the result in the free case (20) and the TF regime (30), respectively, we have

$$\frac{1}{2\hat{a}} = 9.9, \qquad \sqrt{\frac{\hat{b}}{2\hat{a}}} = \pi, \quad (53)$$

and the final $M_c - R$ relation should read

$$M_c = 9.9 \frac{\frac{\hbar^2}{Gm^2 R}}{1 - \pi^2 \frac{3g}{4\pi Gm^2 R^2}}. \quad (54)$$

We stress that this way of obtaining the mass-radius relations for the soliton in this subsection is particularly interesting, because the only thing we needed to do was to consider the characteristic scales of the system. In all cases, this simple analysis reproduces correctly the main features already known from the numerical and analytical descriptions of the soliton; i.e., the relation between $M_c$ and $R_c$ does not depend upon details of the trial function. The only differences which occur involve the numerical values of the constants that accompany the parameter dependence of the different relations, and they are all within factors of a few. Nevertheless, for the sake of concreteness, we decided to continue to use the results obtained earlier from the Gaussian ansatz for the rest of this work.

## B. Implications from a general-relativistic treatment

The analysis of the previous subsections was carried out in the weak-field limit. This limit serves as a good approximation, given that it is very well justified at galactic scales. Yet, it leaves out an important physical phenomenon, namely the fact that a limiting maximum mass is predicted to exist for the soliton, once general-relativistic effects are considered.

It is then natural to anticipate that for certain masses of the soliton, a relativistic treatment should be important—as it turns out, it is possible that some of the cores of SFDM halos are not covered by the weak-field limit, for example, the massive solitonic cores within massive galaxies [see Eq. (4) or the next section for the generalization to the self-interacting case]. In this circumstance, the correct way to model such solitons should be in the general relativistic framework, i.e., by solving the EKG system (5). For this reason, in this subsection, we review an important consequence obtained when relativistic effects are taken into consideration: the maximum mass beyond which the soliton will collapse to form a BH.

By analogy to the weak-field limit, we assume that the core profiles in the central region of galactic halos made of SFDM are given by the minimum-energy, coherent, quasistationary solution of the EKG system (5). We can obtain such solutions by demanding spherical symmetry. In this case, the spacetime for the self-gravitating scalar field can be well described by the metric

$$ds^2 = -\alpha(r)^2 dt^2 + a(r)^2 dr^2 + r^2 d\Omega^2, \quad (55)$$

where $\alpha$ and $a$ are real metric functions, $r$ is usually called areal radius, and $d\Omega^2 \equiv d\theta^2 + \sin^2\theta d\phi^2$ is the solid angle square differential. [In fact, the limit procedure is shown in Ref. [66], where a standard post-Newtonian treatment reduced the EKG system (5), with a geometry defined by the above metric, to the GPP equations (16)].

The set of equations (5) together with the metric (55) have been extensively studied in the literature in the context of BSs. The procedure by which these BSs can be constructed is similar to that in the Newtonian case (see Ref. [84] for a review and references therein); i.e., a harmonic time dependence for the scalar field is proposed, a central scalar field value $\varphi(0)$ is specified, and the same kind of boundary conditions for the soliton solution than in the weak-field limit are imposed. In doing so, the final configurations that are obtained can be split into two regions—a stable[7] and an

---

[7]The soliton profiles emerging from the weak-field limit are part of this branch. Although the Newtonian approximation makes it appear as if it is possible to construct solitons with unlimited mass, it is important to realize that, within the Newtonian description, there exists a critical value of the parameter $\gamma$ beyond which it is not possible to construct solitons from the scaling property (17). This maximum value is a result of the post-Newtonian treatment of the EKG, and it is associated with the condition of weak gravity.

unstable branch—divided by a maximum mass $M_{c,\max}$ allowed by a BS made of scalar field.[8] The stable branch is at higher radii (i.e., right side of maximum mass), while the unstable branch is at the left side of the maximum mass at smaller radii. For masses bigger than $M_{c,\max}$, stable BSs do not exist, and in such a case, configurations with masses $M > M_{c,\max}$ should collapse to form a BH. The parameter dependence of the maximum mass in the free and repulsive self-interacting models is as follows:

(i) In the free case [66–72],

$$M_{c,\max} \simeq 0.633 \frac{m_{\mathrm{pl}}^2}{m}. \qquad (56)$$

(ii) In the case of a scalar field with repulsive interaction, the maximum mass for stable configurations is given by [85]

$$M_{c,\max} \simeq 0.22\sqrt{\hat{\Lambda}} \frac{m_{\mathrm{pl}}^2}{m}. \qquad (57)$$

Let us compare these results with ours from our ansatz. We may assume that the Gaussian will collapse into a BH, once $R_{99} = 2.38167 R_c \simeq R_{\mathrm{sch}}$, where $R_{\mathrm{sch}} \equiv 2M_c G/c^2$ is the Schwarzschild radius associated with the soliton. By considering (29), expressing hat quantities in terms of physical ones with (15) and equating $R_{99} = R_{\mathrm{sch}}$, we obtain in the free case $M_{c,\max} \simeq 2.11 \, m_{\mathrm{pl}}^2/m$, whereas in the strongly repulsive self-interaction regime, $M_{c,\max} \simeq 3.57\sqrt{\hat{\Lambda}} m_{\mathrm{pl}}^2/m$. Note that in both cases, the same parameter dependence is maintained for $M_{c,\max}$ as for the general-relativistic results, with the only difference again in the numerical prefactors that accompany each relation. Of course, the difference between these prefactors is rooted in the fact that we are trying to match a Newtonian ansatz with a general-relativistic result[9] and, as expected, the critical masses from general relativity are lower than the results from the weak-field limit suggest.

Whatever SFDM regime we consider, once the soliton has a mass which ever-so-slightly exceeds its limiting maximum mass, the soliton will collapse to form a BH.

---

[8]The way to know if a configuration will have a given dynamics proceeds by calculating the binding energy of the BS as $E_b = M_{\mathrm{MS}}(r \to \infty) - Nm$, where $M_{\mathrm{MS}}$ is the mass of the BS enclosed within a given $r$, defined in terms of the Misner-Sharp mass function $M_{\mathrm{MS}} = \frac{r}{2}(1 - \frac{1}{a^2(r)})$, and $N$ is the total number of bosons. It happens that when $E_b > 0$, the system has an excess of energy and will disperse. On the other hand, if $E_b < 0$, the system is gravitationally bound and will collapse to a BH, if it is in the unstable branch. Otherwise, it will remain coherent, if it is in the stable branch.

[9]We should expect differences, first by the fact that we are comparing a Newtonian result with a general-relativistic result but also because we are assuming an ansatz solution, which differs from the exact Newtonian treatment (without ansatz).

In order to simplify our descriptions, we will henceforth use the term maximum mass of soliton and critical BH collapse mass (meaning that this is the minimum mass at which a BH could be formed in this scenario) synonymously, because the value of the latter is basically the same as that of the former. Since we are interested in correct orders of magnitude estimates, this little distinction is not critical.

## IV. CORE-HALO STRUCTURE IN SELF-INTERACTING SFDM

The numerical simulations performed by several authors [19,31–37] have revealed that halos made of SFDM without self-interaction show a core-envelope structure, where a central core transitions at a certain radius to an "NFW-like" halo envelope.

Several attempts have been made to understand whether there are global relationships that allow the quantities of these central solitons to be related to properties of the halo. However, the correct way in which they are related is not yet fully understood, as several of these works have reported different functional relations between the masses of these cores and the total halo. For example, in Refs. [19,31], it is reported from cosmological simulations a core-halo mass relation, which we can write in a fiducial way as

$$M_{c,7} \simeq 1.4 \times 10^2 \frac{M_{h,12}^{1/3}}{m_{22}}, \qquad (58)$$

where

$$M_{h,12} \equiv M_h/(10^{12} \, M_\odot)$$

and the subindex $h$ refers to halo quantities. References [19,31] also show that in all the galaxies that they simulated, the final structures also fulfilled the energy relation

$$M_c \simeq 4.3 \sqrt{\frac{|E_h|}{M_h}} \frac{m_{\mathrm{pl}}^2}{mc}. \qquad (59)$$

Several authors (see, for example, Refs. [34,86,87]) have reasoned that the above core-halo mass relationship could be explained, if the characteristic circular or virial velocity at the core radius is roughly the same order as that at the halo radius ("velocity dispersion tracing"), i.e., that the condition

$$v_c \sim v_h \Rightarrow \frac{GM_c}{R_c} \sim \frac{GM_h}{R_h} \qquad (60)$$

should be fulfilled. The physical meaning of this relation is that the size of the soliton matches the de Broglie wavelength, expressed with the velocity dispersion $\sigma$ of the halo,

resulting in a nontrivial type of nonlocal uncertainty principle; it has been also suggested that this relation follows from an equilibrium between the virial temperature of the core and the halo. On the other hand, in Ref. [76], it was suggested that, for an isolated soliton whose mass is written as Eq. (22a), and comparing with the result of Ref. [31], Eq. (59), the core-halo mass relation could be understood, if the specific energy for the central soliton and for the host halo are the same, i.e., if the condition

$$\frac{|E_c|}{M_c} \simeq \frac{|E_h|}{M_h} \qquad (61)$$

applies. Observe that, from the virial theorem for a free SFDM particle, the above condition also implies that

$$\frac{K_c}{M_c} \simeq \frac{K_h}{M_h}. \qquad (62)$$

In a more recent work, in Ref. [77], it is suggested that the latter relation was better suited to reproduce core-halo relations. However, so far, all of these three relations are being used in the literature to explain the physical nature of (58). This is because, in the free case, these three expressions reduce to the same thing. This can be easily seen as follows: suppose that the core is in virial equilibrium, fulfilling

$$2K_c + W_c = 0. \qquad (63)$$

Next, we assume that the halo itself also fulfils his own virial equilibrium, i.e.,

$$2K_h + W_h = 0. \qquad (64)$$

Of course, we might question in which sense it is meaningful to assume separate virial equilibrium, for the core and for the halo. In practice, the above relationships will only hold approximately, especially for the halo, which takes a longer time to virialize, during which time the core might have already virialized. From (63), we have

$$\frac{K_c}{M_c} = -\frac{1}{2}\frac{W_c}{M_c}, \qquad (65)$$

and (64) implies

$$\frac{K_h}{M_h} = -\frac{1}{2}\frac{W_h}{M_h}. \qquad (66)$$

Combining the above relationships and Eq. (62) and using expressions for the potential energy,

$$W_c = -C_{\mathrm{grav}}^{(c)}\frac{GM_c^2}{R_c}, \qquad W_h = -C_{\mathrm{grav}}^{(h)}\frac{GM_h^2}{R_h}, \qquad (67)$$

with positive constants $C_{\mathrm{grav}}^{(c)}$ and $C_{\mathrm{grav}}^{(h)}$ of order 1, which depend upon details of the core and halo profiles, respectively, this yields

$$C_{\mathrm{grav}}^{(c)}\frac{M_c}{R_c} \simeq C_{\mathrm{grav}}^{(h)}\frac{M_h}{R_h}. \qquad (68)$$

Observe that the above expression is equivalent to (60). Despite this "coincidence," we must emphasize that it cannot be expected to be true more generally, once contributions from extra terms (as is the case of a self-interaction between particles) are added to the system [compare (35a) or (35b) with $v_c$ in (60), for example].

On the other hand, in Ref. [34], a different result was reported, compared to Refs. [19,31]. In the simulations of Ref. [34], noncosmological but fully virialized, they obtain a core-halo mass relation in the form

$$M_c \sim M_h^{5/9}. \qquad (69)$$

Reference [34] also reported an empirical relation for their results, given by

$$M_c \simeq 2.6\left(\frac{|E_h|}{(mG/\hbar)^2}\right)^{1/3}, \qquad (70)$$

which can be also reexpressed, using the virial theorem (14) in the free case as

$$M_c \simeq 2.6\left(\frac{K_h}{(mG/\hbar)^2}\right)^{1/3} = 2.6\left(\frac{|W_h|}{2(mG/\hbar)^2}\right)^{1/3}. \qquad (71)$$

It is worth mentioning that these results have been reproduced by more authors, even in a cosmological context (see, for example, Ref. [36]), different from those reported in Refs. [19,31]. However, as Ref. [76] realized, the finding of Ref. [34] in Eq. (70) can be understood, if the condition $E_c \simeq E_h$ applies [compare, for example, Eqs. (70) and (22b)], which from the virial theorem in the free case should be equivalent to $K_h \simeq K_c$ or $W_h \simeq W_c$. This suggests that the halos generated in the simulations of Ref. [34] were dominated by the central soliton. Therefore, a more general scenario may mandate a relation like

$$M_c v_c^2 \sim M_h v_h^2 \qquad (72)$$

or, in other words, the square of the circular or virial velocity at the core radius would differ by a factor of $(M_h/M_c)$ from the one that is measured at the halo radius. Notice that this last conclusion is not limited to assuming that the halos were mostly dominated by the soliton.

Now, in this section, we are interested in extending the core-halo mass relation to SFDM models with self-interaction. A question that immediately arises before we proceed concerns the correct relation upon which we shall

build our extension. Since it appears as if more simulation work will be required to settle this question, we will go ahead and work out an extension for each of the reported core-halo mass relations. This way, we can also clearly see which analytic premises are the basis of each relation, reported either in Refs. [19,31] or Ref. [34].

To begin with, it is necessary to be able to obtain quantities related to the entire halo. For our purposes and the scales of interest, it is sufficient to assume a halo with approximately constant density. In that case, all the energies defined in (11b) and (13) can be expressed as

$$E_t(R) = -\frac{3G}{10}\frac{M^2(R)}{R} - \frac{3g}{8m^2\pi}\frac{M^2(R)}{R^3}, \qquad (73a)$$

$$K_t(R) = \frac{3G}{10}\frac{M^2(R)}{R} - \frac{9g}{8m^2\pi}\frac{M^2(R)}{R^3}, \qquad (73b)$$

$$W_t(R) = -\frac{3G}{5}\frac{M^2(R)}{R}, \qquad (73c)$$

$$U_{SI,t}(R) = \frac{3g}{4m^2\pi}\frac{M^2(R)}{R^3}, \qquad (73d)$$

where in the above expression we have integrated from 0 to a given $R$. If we use the definition of the virial mass of the halo as $M_h = 4\pi R_h^3 \rho_{200}/3$, where $R_h$ is the radius within which the mean density $\rho_{200}$ is 200 times larger than the background density, then from the above expressions follows

$$E_h = -\left[\frac{3}{10}\frac{GM_{\text{crit}}^{1/3}}{R_{\text{crit}}}M_h^{5/3} \pm \frac{1}{4}\frac{GM_{\text{crit}}}{R_{\text{crit}}}M_h\right], \quad (74a)$$

$$K_h = \left[\frac{3}{10}\frac{GM_{\text{crit}}^{1/3}}{R_{\text{crit}}}M_h^{5/3} \mp \frac{3}{4}\frac{GM_{\text{crit}}}{R_{\text{crit}}}M_h\right], \quad (74b)$$

$$W_h = -\frac{3}{5}\frac{GM_{\text{crit}}^{1/3}}{R_{\text{crit}}}M_h^{5/3}, \qquad (74c)$$

$$U_{SI,h} = \pm\frac{1}{4}\frac{GM_{\text{crit}}}{R_{\text{crit}}}M_h, \qquad (74d)$$

where we have defined the quantity $M_{\text{crit}} \equiv 4\pi\rho_{200}R_{\text{crit}}^3/3$ and we have used again the critical radius $R_{\text{crit}} = \sqrt{6|g|/(4\pi Gm^2)}$. From these last expressions, we can already begin to infer several possible consequences regarding our extensions. On the one hand, we can see that if the total halo is in the TF regime ($K_h \simeq 0$), from Eq. (74b), we arrive at $R_h \simeq R_c^{(\text{TF})}$. Of course, this is unfavorable because it implies that we have one size for all halos in the Universe, and halos would effectively be limited to solitonic cores in the TF regime.

Therefore, any possible extension for models with self-interaction that pretends to maintain an NFW-like asymptotic exterior would necessarily have to consider a kinetic term, different from zero, to describe the complete halo. Since SFDM is expected to behave like CDM at large scales (i.e., scales much larger than either the de Broglie wavelength in the free case or much larger than the TF radius in the TF regime), it should be true that at sufficiently large galactic scales, CDM should be recovered, suggesting that these NFW envelopes should be also found, even in the TF regime. On the other hand, observe that the total energy of the halo can be expressed as

$$E_h \sim -\left(\frac{3}{10}R_h^5 \pm \frac{1}{4}R_{\text{crit}}^2 R_h^3\right), \qquad (75)$$

so if we demand that $R_h \gg R_{\text{crit}}$, we can express the total energy of the system as

$$E_h \simeq -\frac{3}{10}\frac{GM_{\text{crit}}^{1/3}}{R_{\text{crit}}}M_h^{5/3}. \qquad (76)$$

Notice that the above expression results in $E_h \sim W_h \sim GM_h^2/R_h$, even if self-interaction is allowed for the SFDM particles. On the other hand, from (35a), the energy for the soliton would be always in the range

$$\frac{1}{4\sqrt{2\pi}}\left(\frac{GM_c^2}{R_c}\right) \le |E_c| \le \frac{1}{3\sqrt{2\pi}}\left(\frac{GM_c^2}{R_c}\right), \qquad g > 0,$$

$$\frac{1}{6\sqrt{2\pi}}\left(\frac{GM_c^2}{R_c}\right) \le |E_c| \le \frac{1}{4\sqrt{2\pi}}\left(\frac{GM_c^2}{R_c}\right), \qquad g < 0,$$

and similar relations for $W_c$, meaning that $|E_c| \sim |W_c| \sim GM_c^2/R_c$ in all cases. With this simple analysis, we can conclude that the extensions that follow from the relations (60) from the results of Refs. [19,31] or (72)[10] from the results of Ref. [34] should be sufficient to capture realistic results for our self-interaction models.

## A. Extending the core-halo mass relation, using the results of Refs. [19,31]

Now, let us study the consequences, once we assume that Eq. (60) is the correct basis for the extension of the core-halo mass relation in SFDM. Recently, an extension was also considered in Ref. [86], modeling the total halo with a generalized GPP system [88], obtaining that the total halo could be understood as a central soliton with an effective isothermal exterior. Nevertheless, we proceed to present here our own extension by following the procedures that we

---

[10]Observe that by adopting this relation we are also assuming that the results obtained in Ref. [34] are general and apply in cases for which the mass of the central soliton is much smaller than the mass of the total halo.

have applied so far. For this purpose, we assume that the core-halo mass relation, that we seek, is based upon the condition

$$\frac{GM_c}{R_c} \simeq D_h \frac{GM_h}{R_h}, \tag{77}$$

where $D_h$ is a constant that must be fixed by numerical simulations. On the other hand, it is not difficult to rewrite the $M_c - R_c$ relation for the Gaussian ansatz as

$$M_c = (3\sqrt{2\pi})^{1/2} \frac{m_{\mathrm{pl}}^2}{m} \frac{\sqrt{\frac{GM_c}{R_c}}}{c} \sqrt{1 + \sqrt{\frac{2}{\pi}}\hat{\Lambda} \frac{\left(\frac{GM_c}{R_c}\right)}{c^2}}. \tag{78}$$

We can express the above equation in terms of halo quantities using Eq. (77). If additionally we replace $R_h = (3M_h/4\pi\rho_{200})^{1/3}$, we obtain that the mass of the core can be expressed in terms of the mass of the complete halo as

$$M_c = \frac{m_{\mathrm{pl}}^2}{m} \sqrt{3\sqrt{2\pi}\hat{D}_h M_h^{2/3}\left(1 + \sqrt{\frac{2}{\pi}}\hat{\Lambda}\hat{D}_h M_h^{2/3}\right)}, \tag{79}$$

where in the above expression we have defined $\hat{D}_h \equiv (4\pi\rho_{200}D_h^3 G^3/(3c^6))^{1/3}$. Finding the numerical value of $\hat{D}_h$ by matching the above expression with $\hat{\Lambda} = 0$ and the core-halo mass relation in the free case, Eq. (58), we finally arrive at our core-halo mass relation in fiducial units:

$$M_{c,7} = \frac{1.4 \times 10^2 M_{h,12}^{1/3}}{m_{22}} \sqrt{1 + \hat{\Lambda}(1.16 \times 10^{-7} M_{h,12}^{2/3})}. \tag{80}$$

To understand the consequences that follow from the above result, we plot in Fig. 2 $M_c$ (top panel), $R_c$ (middle panel), and $\bar{\rho}_c \equiv 3M_c/(4\pi R_c^3)$ (bottom panel) as a function of $M_h$ setting $m_{22} = 1$. Observe that, from this extension, we obtain that for attractive SFDM, there is a critical halo mass,

$$M_{h,12}^{(\mathrm{crit})} = \left(\frac{4.29 \times 10^6}{|\hat{\Lambda}|}\right)^{3/2}, \tag{81}$$

at which the central soliton arrives at its maximum possible mass

$$M_{c,7}^{\max} = \frac{2.05 \times 10^5}{m_{22}|\hat{\Lambda}|^{1/2}}. \tag{82}$$

This maximum mass is indicated as the red square in the plot. It is not difficult to show that the above expression coincides with (31) once rewritten in appropriate units. On the other hand, when $\hat{\Lambda} > 0$ and
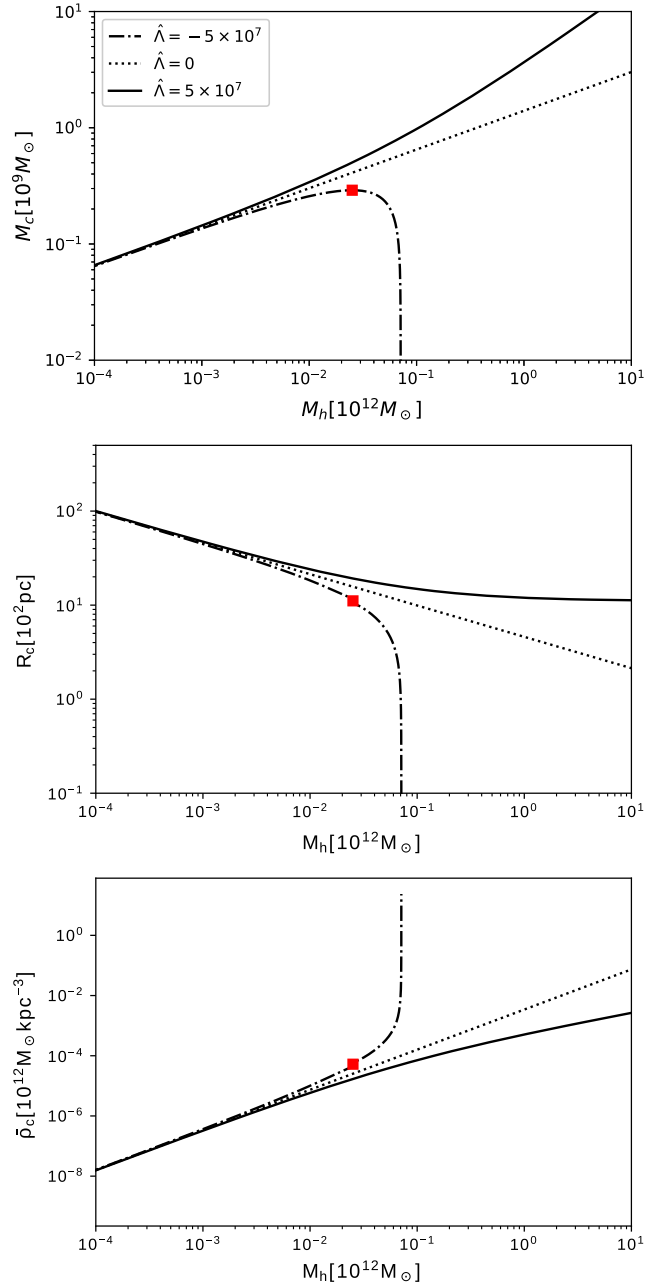


FIG. 2. Mass, radius, and mean density for a soliton in self-interacting SFDM halos, in terms of total halo mass for our Schive *et al.* [19,31] extension. For the following cases: repulsive self-interaction ($\hat{\Lambda} = 5 \times 10^7$; solid curves), attractive self-interaction ($\hat{\Lambda} = -5 \times 10^7$; dot-dashed), and no self-interaction ($\hat{\Lambda} = 0$; dotted). The red squares labeling the attractive case curves correspond to $M_c^{max}$.

$\hat{\Lambda}(1.16 \times 10^{-7} M_{h,12}^{2/3}) \gg 1$, we arrive at the TF regime for the central soliton profile, resulting in a core-halo mass relation in the form

$$M_{c,7} \simeq 4.78 \times 10^{-2} \frac{\sqrt{\hat{\Lambda}}}{m_{22}} M_{h,12}^{2/3}. \tag{83}$$

This core-halo mass relation in the TF regime is in agreement with the one obtained in Ref. [86].

### B. Extending the core-halo mass relation, using the results of Ref. [34]

For this extension, we consider the following condition that should correctly describe core-halo quantities,

$$\frac{GM_c^2}{R_c} \simeq C_h \frac{GM_h^2}{R_h}, \tag{84}$$

where, as before, $C_h$ is a constant that must be fixed by numerical simulations. Multiplying Eq. (78) by $M_c$ on both sides, using the above expression and again $R_h = (3M_h/4\pi\rho_{200})^{1/3}$, it is easy to see that the core-halo mass relation is given by the expression

$$M_c^2 = \frac{m_{\rm pl}^2}{m} \sqrt{3\sqrt{2\pi}\hat{C}_h M_h^{5/3}\left(M_c + \sqrt{\frac{2}{\pi}}\hat{\Lambda}\hat{C}_h M_h^{5/3}\right)}, \tag{85}$$

where $\hat{C}_h \equiv (4\pi\rho_{200}C_h^3 G^3/(3c^6))^{1/3}$. Similarly as in our previous extension, we obtain the numerical value of $\hat{C}_h$ by matching (85) with numerical simulations for $\hat{\Lambda} = 0$. In order to do so, we will proceed using Eq. (70) and noticing that once we use (74) in the free case, it can be rewritten as

$$M_c \simeq 2.6\left[\frac{m_{\rm pl}^4}{m^2 c^2}\frac{3}{10}\left(\frac{4\pi\rho_{200}}{3}\right)^{1/3} M_h^{5/3}\right]^{1/3}. \tag{86}$$

If for consistency we use the current mean density of the Universe $\rho_b = 1.5 \times 10^{-7}\ M_\odot{\rm pc}^{-3}$ and $\rho_{200} = 200\rho_b$, we have that the core-halo mass relation obtained in Mocz *et al.* [34] simulations should be roughly given by

$$M_{c,7} \simeq 1.31 \times 10^3 \frac{M_{h,12}^{5/9}}{m_{22}^{2/3}}. \tag{87}$$

Comparing this with (85) in the free case, we obtain finally that the core-halo mass relation with self-interaction corresponds in fiducial units to

$$M_{c,7}^2 \simeq \frac{4.75 \times 10^4 M_{h,12}^{5/6}}{m_{22}}\sqrt{M_{c,7} + \hat{\Lambda}(1.34 \times 10^{-2} M_{h,12}^{5/3})}. \tag{88}$$

Again, we plot $M_c$ (top panel), $R_c$ (middle panel), and $\bar{\rho}_c$ (bottom panel) as a function of $M_{h,12}$ for this case in Fig. 3. Observe that in all cases, this extension leads to larger masses for the central soliton than in the Schive *et al.* [19,31] extension, Eq. (80). This conclusion was also pointed out by Mocz *et al.* for their results of the free case. In addition, similarly to the other extension, there is a critical total halo mass for attractive SFDM,
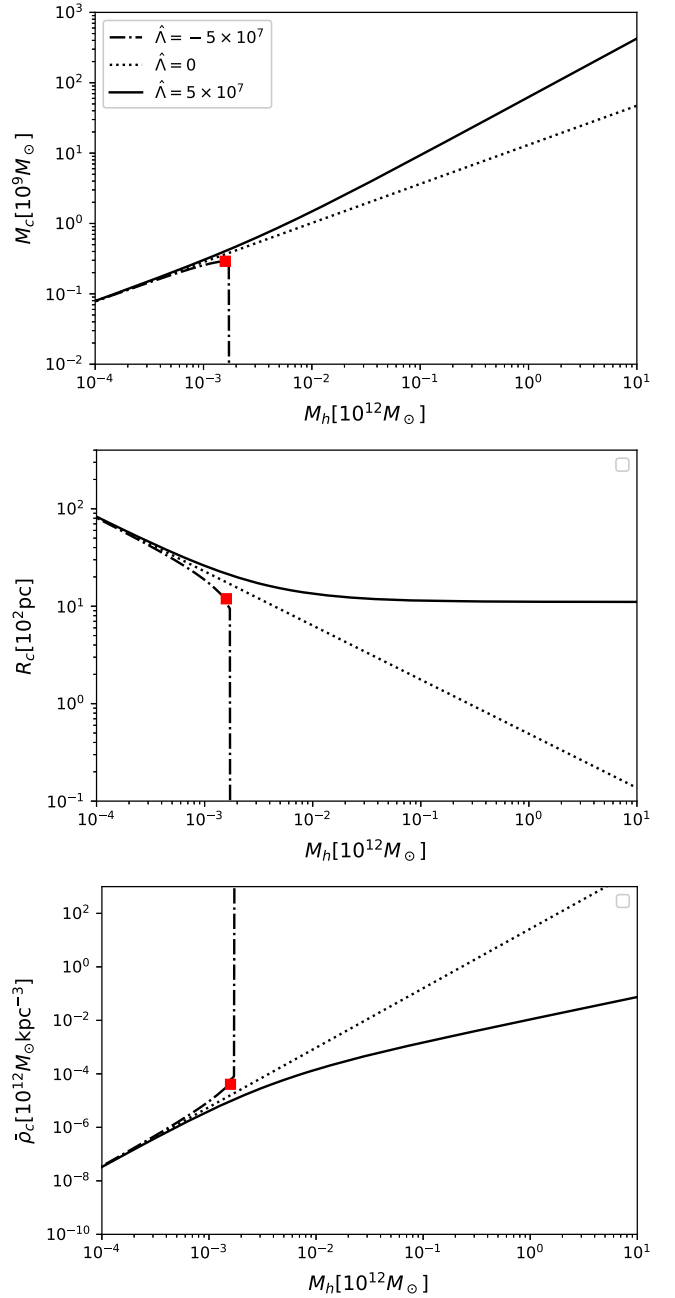


FIG. 3. Same as Fig. 2, except for our Mocz *et al.* [34] extension, instead. Note that the curves for the attractive case have a steeper inflection point than before, as a result of the different power-law dependency.

$$M_{h,12}^{\rm (crit)} = \frac{1.34 \times 10^4}{(m_{22}|\hat{\Lambda}|^{3/2})^{3/5}}, \tag{89}$$

at which the central soliton arrives at its maximum possible mass; the latter is again indicated as the red square in the plot. It is found by inserting (89) in Eq. (88); we arrive at the same result as in Eq. (82), which, as we explained before, is just the same as (31) but rewritten in our fiducial units. (Note that the different "x-axis" coordinates of the

red square between Figs. 2 and 3 reflect the different core-halo mass extensions.) On the other hand, when $\hat{\Lambda} > 0$ and $\hat{\Lambda}(1.34 \times 10^{-2} M_{h,12}^{5/3}) \gg M_{c,7}$, we arrive at the TF regime, in which the core-halo mass relation in this limit is given by

$$M_{c,7} \simeq 74.15 \left( \frac{\sqrt{\hat{\Lambda}}}{m_{22}} \right)^{1/2} M_{h,12}^{5/6}. \qquad (90)$$

## V. ASTROPHYSICAL CONSEQUENCES FOR SFDM WITH SELF-INTERACTION

A fundamental question that arises in the SFDM model concerns the values of its free parameters. Many constraints have been derived already, using cosmological and astrophysical data. In this section, we first review some of the most representative results obtained in the literature and apply them to our extensions; i.e., we shall confront our extensions obtained, using the simulation results of Schive *et al.* [19,31] and those of Mocz *et al.* [34].

In particular, we will confront the parameter space of SFDM and our core-halo mass extensions by exploring the possibility of SMBH formation in each scenario. As we have seen, this question immediately arises, once we realize that solitonic cores have limiting maximum masses, beyond which they collapse to a BH, in light of the core-halo mass relations of SFDM halos. Again, we remind the reader that in order to simplify our descriptions, we will use the term maximum mass of soliton and critical BH collapse mass synonymously, because the value of the latter is basically the same as the former.

We will also comment on other consequences that arise, once we confront the parameter region that has been studied by other observational data.

As we already mentioned, SMBHs with masses in the range $M_{\text{SMBH}} \simeq 10^6 – 10^{10} \ M_\odot$ have been found in almost all large galaxies, while this is not the case for the smallest ones, like dwarf spheroidals (dSphs). However, BHs of masses around $10^6 \ M_\odot$ have been found in some dwarf galaxies, e.g., Ref. [89], while Ref. [90] has reported BHs with smaller masses of $10^4 – 10^5 \ M_\odot$ in dwarf galaxies, albeit this nondynamical mass estimate is very much uncertain.[11] Thus, we could try to find scenarios in which the central solitons reach their maximum possible mass only for the most massive galactic halos (hosting the most massive galaxies). However, it is unclear at this point whether the core-halo mass relations found in current simulations of free SFDM—on which we based our extensions—remain valid for the most massive galactic-size halos, because all these simulations were limited to

---

[11]Also, recently, a BH has been detected in the intermediate mass range with a mass of approximately $150 \ M_\odot$, generated by the merger of two smaller BHs [91]. Of course, our intention in this work is only to explain the SMBHs within galactic nuclei, so the formation of these objects is not covered by our models.

small volumes. Therefore, it seems appropriate to apply the core-halo mass relations to the question of SMBH formation in halos whose critical mass for soliton collapse, $M_{h,12} = M_{h,12}^{(\text{max})}$, does not exceed a certain limit, which we choose to set at 1 (in these units). We may think of the resulting SMBHs as the "seeds" for possibly even more massive SMBHs in the centers of the most massive galaxies.

For consistency with observations, however, the mass of these SMBH seeds would be expected to not exceed the mass of the least massive SMBHs found in galaxies, as, e.g., in our own Milky Way, which harbors a SMBH of approximately $4 \times 10^6 \ M_\odot$. We could also assume that these SMBH seeds could be orders of magnitude smaller but that mass range would fall into the so-called intermediate mass range, which is still under debate, as mentioned above. Therefore, we will only focus on SMBH seeds that are still in the supermassive range. More precisely, we will consider a fiducial mass range of such seed SMBHs, equivalently to consider a range for the maximum mass of solitonic cores of $M_{c,7}^{\text{max}} \simeq 0.1–10$, whose collapse is supposed to form these SMBHs. Similarly, we need to take fiducial values for $M_{h,12}^{(\text{crit})}$ such that these SMBHs are not formed for the least massive galaxies, such that they keep having a stable soliton core in their centers, nor for very large galaxy/halo masses, as explained above. In analogy to the above description, we could expect that this critical mass of collapse corresponds to the minimum mass of a galactic halo in whose center the presence of a SMBH is expected; however, we decided again to be flexible, and we adopted as a conservative criterion that galactic halos with masses in the range $M_{h,12}^{(\text{crit})} \simeq 10^{-2} - 1$ are the ones that will "start" to possess a SMBH at their center. In what follows, we will call the combination of these two ranges of fiducial parameters (when both are met simultaneously) our "ideal model," where, of course, it is understood that we refer to this ideal model only in the context of the formation of these seeds in the supermassive range.

### A. Free case ($\hat{\Lambda} = 0$)

This is the best-studied case in the literature and several constraints have been found by different groups for this model. Here, we shall review only some representative constraints.

Using the hydrodynamical representation of the SFDM model, it was suggested in Ref. [92] that the quantum pressure of SFDM explains the offset between DM and ordinary matter in galaxy cluster Abell 3827. For this purpose, a mass of $m_{22} \simeq 2 \times 10^{-2}$ was required. When the model is tested with the dynamics of dSphs—Fornax and Sculpture—in Ref. [93], a mass constraint of $m_{22} < 0.4$ at 97.5% was obtained. The constraints which follow when the survival of the cold clump in Ursa Minor and the

distribution of globular clusters in Fornax is demanded, requires a mass $m_{22} \sim 0.3\text{–}1$ [94]. Explaining the half-light mass of ultrafaint dwarfs requires $m_{22} \sim 3.7\text{–}5.6$ [95]. The model has been also constrained by reionization: in Ref. [96], using N-body simulations and demanding an ionized fraction of HI of 50% by $z = 8$, $m_{22} > 0.26$ was obtained. Finally, the Lyman-$\alpha$ forest flux power spectrum stands out from the rest in demanding a comparatively high upper bound of $m_{22} \geq 20\text{–}30$ [97,98].

Here, we probe the possibility of formation of SMBHs for free SFDM, in light of the discussion of the beginning of this section. For this case, it is sufficient to apply the results obtained by Schive *et al.* (58) and Mocz *et al.* (87).

Observe that by equating the core-halo mass relation (58) and the critical mass of collapse (56) for a soliton in the free case, which in fiducial units reads

$$M_{c,7}^{\max} = \frac{8.46 \times 10^4}{m_{22}}, \tag{91}$$

we obtain that the maximum possible soliton mass is reached for a critical halo mass of

$$M_{h,12}^{(\mathrm{crit})} \simeq 2.204 \times 10^8. \tag{92}$$

This value exceeds by many orders of magnitude even the halos around the most massive galaxies with $M_{h,12} \sim 10^2$. Interestingly, this result is independent of the mass of the SFDM particle. Therefore, we find that the core-halo mass relation due to Schive *et al.* [19,31] implies that the formation of SMBHs by soliton collapse is not possible.

Now, we can proceed in the same way with equation (87) and (91). In this case, we obtain that the critical halo mass at which the central soliton arrives at its maximum possible mass is

$$M_{h,12}^{(\mathrm{crit})} \simeq \frac{1.81 \times 10^3}{m_{22}^{3/5}}, \tag{93}$$

i.e., different from (92). In fact, if we adopt the core-halo mass relation of Mocz *et al.* [34] as the correct one, we do have scenarios in which the central soliton in galaxies can collapse and form a SMBH for some values of the mass parameter of SFDM. In order to highlight what the values for the mass parameter must be in order to achieve soliton collapse, we plot in Fig. 4 $M_{h,12}^{(\mathrm{crit})}$ [Eq. (93); left "y" axis] and $M_{c,7}^{\max}$ [Eq. (91); right y axis] with a dot-dashed black line as a function of $m_{22}$. To understand better how this figure should be read, let us focus on a special case, for example, the case for which $m_{22} = 1$. In Fig. 4, we plot this case with a red vertical line. Observe that this line intersects in some point with the dot-dashed black line. It is precisely at this intersection where we can talk about the critical masses $M_{h,12}^{(\mathrm{crit})}$ and $M_{c,7}^{\max}$ that correspond to this particular example. To know exactly what these masses are,
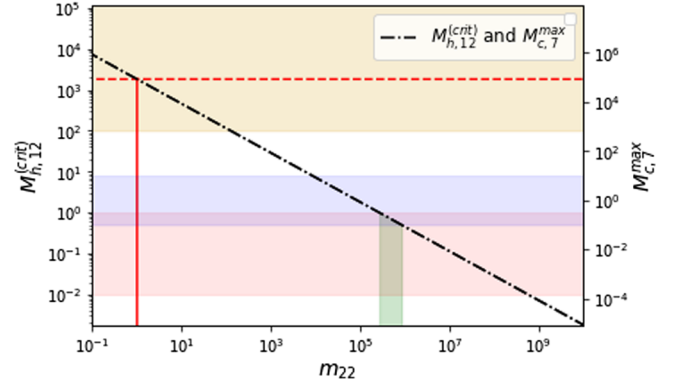


FIG. 4. $M_{h,12}^{(\mathrm{crit})}$ (left y axis) and $M_{c,7}^{\max}$ (right y axis) as a function of $m_{22}$ (dot-dashed line). The blue and red bands correspond to our fiducial values $M_{c,7}^{\max} = 0.1\text{–}10$ and $M_{h,12}^{(\mathrm{crit})} = 10^{-2} - 1$, respectively, whereas the green region represents the parameter range in $m_{22}$ that fulfils the ideal model, i.e., as a result of the above fiducial choice. The golden band (upper part in the plot) indicates the range $M_{h,12}^{(\mathrm{crit})} > 10^2$ of galactic halos whose mass is excluded by observations (see the main text for more explanations).

the reader may just look at the horizontal dashed red line and the point at which it intersects both y axes; i.e., for the special case of $m_{22} = 1$, we obtain that galaxies with a critical mass $M_{h,12}^{(\mathrm{crit})} = 1.81 \times 10^3$ should possess a soliton with a mass that equals its maximum possible mass $M_{c,7}^{\max} = 8.46 \times 10^4$.

Clearly, this example is far away from belonging to our ideal model. Therefore, we draw in blue and red the fiducial mass ranges of our ideal model, i.e., $M_{c,7}^{\max} = 0.1\text{–}10$ and $M_{h,12}^{(\mathrm{crit})} = 10^{-2} - 1$, respectively. The first thing we can observe from these two bands is that they only overlap in a small region, which corresponds to having collapse with critical masses of $M_{c,7}^{\max} = 0.31\text{–}0.1$, once the mass of the galactic halo exceeds the corresponding critical values $M_{h,12}^{(\mathrm{crit})} = 0.5\text{–}1$. This overlap coincides with values of the mass parameter in the range $m_{22} = 2.69 \times 10^5\text{–}8.46 \times 10^5$ (green region in the plot). This implies that we could meet our ideal model only for this range of parameters, implying that if we were interested in explaining the possible formation of SMBHs, the range $m_{22} = 2.69 \times 10^5\text{–}8.46 \times 10^5$ would be favored. Let us explain in more detail why we consider these masses as the ones that are favored. Suppose our ideal model is only partially fulfilled. For example, if we try to meet the condition of obtaining collapse, once we reach critical halo masses of $M_{h,12}^{(\mathrm{crit})} = 10^{-2} - 1$, it would result in the formation of SMBH seeds from solitons with $M_{c,7}^{\max} \simeq 1.46 \times 10^{-4}\text{–}3.15 \times 10^{-1}$, so the mass of most of the resulting SMBH seeds would be well below the mass of typical SMBHs found in galactic nuclei, and instead they

would correspond to intermediate mass BHs. Since we do not consider the intermediate mass range in our scenario, the only masses that could account for such SMBH seeds would be the most massive ones, those that fall within the overlap region of our ideal model. Similarly, if we require instead meeting the condition of obtaining collapse for soliton masses $M_{c,7}^{max} = 0.1$–$10$, the mass of the galactic halos for which such collapse could be achieved is $M_{h,12}^{(crit)} = 0.5$–$8.07$, leading to a correspondingly high range of halo masses. Although such halo masses do exist in the Universe, we discard the most massive of them (the ones that are not covered by our ideal model), because SMBHs have been observed also in less massive galaxies. So, if we want to explain the latter through this mechanism, we require them to be formed from smaller critical halo masses.

Finally, we compare our estimates for the particle mass parameter with the constraints that have been found by other groups. Once we make the comparison, we can see that our range of preferred values $m_{22} = 2.69 \times 10^5$–$8.46 \times 10^5$ is completely in disagreement with most of the previous studies. At best, the only agreement can be found with those that follow from reionization and the Lyman-$\alpha$ forest flux power spectrum. Despite this discrepancy, it should be heeded that adopting values for the particle mass of SFDM that are as large as ours would imply that our model increasingly resembles standard CDM, so that the range of parameters that we are taking for our ideal model cannot be ruled out as of yet, if we accept the notion that CDM has not yet been ruled out. In that case, of course, SFDM with such model parameters would not resolve the CDM small-scale crisis, either, but instead, it could help to explain SMBH formation (a feature not directly predicted by CDM), which makes it an appealing dark matter candidate, again. By the same token, our model can help us to turn the question around and demand to put some extra bounds on the particle mass parameter of SFDM. It is clear that we should avoid making SMBHs of the wrong mass and/or for the wrong halo masses. As we have mentioned before, if SMBHs with masses smaller than supermassive were generated (in the intermediate range), there would be a problem because these BH populations have not yet been firmly detected. That way, we could partially discard this parameter region ($m_{22} > 8.46 \times 10^5$). On the other hand, if we have soliton collapse for galactic halos that are more massive than our fiducial model, we could also rule out that parameter region since, as we mentioned earlier, this is not desirable if we want to use this mechanism to explain the presence of SMBHs in galaxies with smaller masses. If we assume that typically the most massive galactic halos have a mass of the order of $M_{h,12} \simeq 10^2$, the above condition rules out the region $m_{22} = 1.25 \times 10^2$–$2.69 \times 10^5$.

Finally, demanding *nonformation* of SMBHs by this mechanism would also give us a region of allowed parameters for this model. If we demand that for a mass $M_{h,12}^{(crit)} = 10^2$ the critical mass for collapse of the soliton has not yet been reached (marked by the golden band in Fig. 4), we get that the mass parameter of the model should meet the condition $m_{22} \leq 1.25 \times 10^2$. As such, this last constraint does agree with all those that have been previously reported.

## B. Repulsive case ($\hat{\Lambda} > 0$)

This model has been also extensively studied in the literature, and its free parameters have been fit, using different observations. Usually, the strong self-interaction regime is considered, because of simplicity, and in this case, it is the ratio $g/(m^2c^4)$ which is subject to constraints. Observe that, from (15), we have

$$\hat{\Lambda} = 1.54 m_{22}^2 \times 10^{37} \left( \frac{g}{m^2c^4} \right) \frac{eV}{cm^3}; \qquad (94)$$

i.e., we can likewise constrain $\hat{\Lambda}$. In this section, we shall only use the constraints that have been found in the strong self-interaction regime, for one thing, because the bounds are stronger and may hold for weak self-interaction, as well. It is these bounds which will be put into context to our results.

The first constraint, applicable to all candidates for dark matter, refers to the fact that by the redshift of radiation-matter equality $z_{eq}$, they must all be nonrelativistic, i.e., behaving like a pressureless fluid. It is well known that a scalar field with an arbitrary potential $V(\varphi)$[12] will have a varied dynamics during its cosmological evolution. In particular, the dynamics of SFDM with a repulsive self-interaction has been studied previously and can be briefly summarized as follows [9,99,100]: after inflation, the SFDM energy density behaves either like a cosmological constant ($\rho_\varphi \propto a^0$) or a stiff fluid ($\rho_\varphi \propto a^{-6}$), depending upon whether SFDM is effectively a real or complex field, respectively. This behavior of SFDM is rooted in the *slowly oscillating* phase and is characterized by $\omega^2 \equiv 2c^2 dV/d|\varphi|^2 \ll H^2$. However, in its *fast oscillating* regime ($\omega^2 \gg H^2$), there are two possible branches for SFDM [99,101]. For *weak self-interaction*, SFDM transitions from the stiff phase to the pressureless phase without having a radiationlike behavior in between. This happens, because the first term in the scalar field potential (6) dominates over the second term at the moment of transition from slow to fast oscillation. On the other hand, for *strong self-interaction*, SFDM transitions from the stiff phase to a radiationlike phase, before behaving like a pressureless

---

[12]Here, $\varphi$ is the scalar field that appears in the Klein-Gordon equation and is related to $\psi$ via Eq. (9).

fluid. Demanding that, at $z_{\rm eq}$, SFDM should be in its pressureless phase implies a constraint as follows [99]:

$$\frac{\hat{\Lambda}}{m_{22}^2} \leq 6.18 \times 10^{20}. \qquad (95)$$

This result represents an upper bound for the self-interaction parameter, including the weakly self-interacting regime. This last result is also independent of whether SFDM is real or complex, given that the strong and the weak regimes are applicable to both cases. Hence, the above result is applicable to all SFDM models with a repulsive self-interaction.

On the other hand, the repulsive SFDM model has been also probed by studying the effective number of relativistic degrees of freedom during big bang nucleosynthesis (BBN), $N_{\rm eff,BBN}$ [99]. The analysis was performed in the strongly self-interacting regime for complex SFDM, and it was shown that this scenario can be made in accordance with BBN bounds. Using the allowed $1\sigma$-band on $N_{\rm eff,BBN}$ at that time, it was shown that the ratio $g/(m^2 c^4)$ must fulfill an upper and a lower bound. However, if the lower bound of the $1\sigma$-band on $N_{\rm eff,BBN}$ is relaxed, i.e., if BBN is considered in accordance with the standard value of $N_{\rm eff} = 3.046$, then the ratio $g/(m^2 c^4)$ can be much smaller than the above upper bound suggests, as long as the particle mass $m$ fulfils a corresponding lower bound constraint, which ensures that the stiff-like era ends at an early enough time. This analysis is extended in Ref. [102], to include a scenario where the stochastic gravitational wave background (SGWB) from inflation could be amplified, as a result of the stiff-like behavior of SFDM in the very early Universe, after reheating, when SFDM dominates the mean energy density in the Universe. In this case both SFDM and the inflationary SGWB contribute to $N_{\rm eff,BBN}$. The modified bounds which result effectively shrink the available parameter space of complex SFDM further, but in doing so, the SGWB is boosted to a level where it can be potentially observed by LIGO (see Ref. [102]). However, if the stiff phase ends early enough, such that the SGWB remains negligible, the lower and upper bounds on $g/(m^2 c^4)$ are determined basically again by demanding that SFDM fulfills BBN bounds. An updated value for $N_{\rm eff,BBN}$ has been used in Ref. [102] to derive newer bounds for this case, as well. Using (94), the corresponding bounds read as

$$3.55 \times 10^{19} \leq \frac{\hat{\Lambda}}{m_{22}^2} \leq 6.33 \times 10^{20}. \qquad (96)$$

Interestingly, if we use the above parameters in the TF radius (30), it turns out to be of order $R^{\rm (TF)} \sim$ kpc.

Similarly to the previous subsection, we will now try to see if it is possible to explain SMBH formation for repulsive SFDM. To this end, it will be necessary to use each of our extensions of the core-halo mass relations that we derived in the previous section; that is, we shall probe our extensions (80) and (88). We will consider that the central soliton reaches its maximum possible mass by assuming the already known numerical result (57), which in fiducial units reads

$$M_{c,7}^{\rm max} = 2.94 \times 10^4 \frac{\sqrt{\Lambda}}{m_{22}}. \qquad (97)$$

We may anticipate that this result is valid for those solitons that are well within the TF regime (as we analyzed when we compared our Gaussian ansatz with the numerical results in Sec. III B). For this purpose, we will apply our extensions in the TF limit, i.e., using Eqs. (83) and (90).

Let us start by analyzing the extension that is based upon the results from Schive *et al.* [19,31]. If we compare (83) and (97), we find that the central soliton will collapse above a critical halo mass:

$$M_{h,12}^{\rm (crit)} \simeq 4.82 \times 10^8. \qquad (98)$$

This is close to the value that we obtained for free SFDM in (92), and just like there, this quantity does not depend upon the free parameters of the SFDM particle, $m$ and $\lambda$. Again, through this extension, it is not possible to form SMBHs via soliton collapse, because the required critical halo mass is many orders of magnitude too high.

Now, let us study the extension that is based upon the results which follow from Mocz *et al.* [34]. If we compare (90) and (97), we obtain

$$M_{h,12}^{\rm (crit)} \simeq 1.31 \times 10^3 \left(\frac{\sqrt{\hat{\Lambda}}}{m_{22}}\right)^{3/5}. \qquad (99)$$

In Fig. 5, we plotted $M_{h,12}^{\rm (crit)}$ [Eq. (99); left $y$ axis] and $M_{c,7}^{\rm max}$ [Eq. (97); right $y$ axis] as a function of $\hat{\Lambda}/m_{22}^2$. Similarly as in the free case, we draw in blue and red our choice of fiducial ranges of $M_{c,7}^{\rm max} = 0.1$–10 and $M_{h,12}^{\rm (crit)} = 10^{-2} - 1$, respectively. As before, we end up with a small range of SFDM parameters that can fulfil our ideal model (we marked them in green), which are $\hat{\Lambda}/m_{22}^2 = 1.16 \times 10^{-11} - 4.06 \times 10^{-11}$. Only this region of parameters would be favored for possible SMBH formation.

Finally, we need to confront our estimate for SMBH formation and the previous constraints in the literature. We can see that our estimate is in accordance with the constraints in (95) but would be in disagreement with BBN constraints, unless the latter are relaxed by considering the limit of very weak self-interaction. However, somewhat similar to the free case, this scenario cannot be ruled out *per se*, since this region of parameters
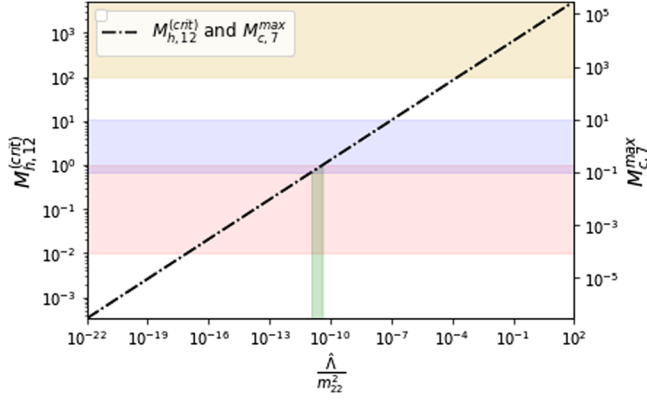
FIG. 5. $M_{h,12}^{(\text{crit})}$ and $M_{c,7}^{\max}$ as a function of $\hat{\Lambda}/m_{22}^2$ (dot-dashed line). The blue, red, golden, and green regions indicate the same meaning as in Fig. 4.

corresponds to having a small TF radius,[13] meaning the model resembles standard CDM. On the other hand, following the same description we did in the free case, we can rule out the region of parameters that pertains to $\hat{\Lambda}/m_{22}^2 < 1.16 \times 10^{-11}$ to avoid the formation of small BH seeds and $\hat{\Lambda}/m_{22}^2 = 4.06 \times 10^{-11} - 1.89 \times 10^{-4}$ to avoid the formation of SMBHs for large halo masses. The requirement of nonformation of SMBHs imposes the condition $\hat{\Lambda}/m_{22}^2 \geq 1.89 \times 10^{-4}$. This last constraint is in agreement with all the previous constraints that we reviewed, if we relax the lower $1\sigma$ bound from BBN.

If we were to adopt this constraint, SMBHs would not form in this scenario, and the core-halo mass relation for this model would be given by Eq. (83) or (90).

*Remark 2.* Observe that we require very small values for $\hat{\Lambda}/m_{22}^2$ in order to explain the possible formation of SMBHs in this model, so we might think that these values should not necessarily be within the TF regime. However, from Eq. (29), we know that the TF regime is reached for $6\hat{\Lambda}(M_{c,7}m_{22}/(5.038 \times 10^5))^2 \gg 1$. If we replace $M_{c,7}$ by $M_{c,7}^{\max}$, this expression imposes the condition

$$\frac{\hat{\Lambda}}{m_{22}^2} \gg \frac{17.14}{m_{22}^2}. \qquad (100)$$

As long as this condition is fulfilled, the model will be in the TF regime.

### C. Attractive case ($\hat{\Lambda} < 0$)

This model is the least studied in the literature in the context of halo formation and dynamics, which is odd given that one of the most promising SFDM candidates is

---

[13]As we have seen in Sec. III A 1, the TF radius can be expressed, using (15) in (30), as $R^{(\text{TF})} \propto \frac{\hat{\Lambda}}{m_{22}^2}$; i.e., a small value of the ratio $\hat{\Lambda}/m_{22}^2$ implies a small TF radius.

axion-like particles. Their attractive self-interaction is often ignored for mere simplicity. So, the constraints of the mass parameter that are obtained in free SFDM are usually shared for these attractive cases, as well. Nevertheless, there has been some work on the effects of an attractive self-interaction, and a few observations are used to put limits on this parameter. The constraints that are found for the self-interaction parameter are usually imposed on the parameter $\lambda$; however, we can reexpress them in terms of $\hat{\Lambda}$ by using (15) as

$$\hat{\Lambda} = 5.93 \times 10^{98} \frac{\lambda}{m_{22}^2}. \qquad (101)$$

The evolution of the background Universe of this model was studied in Ref. [103]. If the SFDM particle is an ultralight axion-like particle ($m_{22} \sim 1$)—a pseudo–Nambu-Goldstone boson generated by a spontaneously broken global $U(1)$ symmetry—it was suggested in Ref. [104] that these particles should be generated during the inflationary epoch in order to avoid observational constraints from Planck data, due to topological defects. There, it was also argued that by demanding that the total DM observed today is composed of these ultralight axions, they should have a self-interaction parameter[14] $|\hat{\Lambda}| \sim 5.93 \times 10^4$, although the value of this self-interaction term can increase, as long as the value of $m$ also increases. These axion-like particles have also been studied in the context of type IIB orientifold compactifications in string theories, resulting in the possibility of obtaining stronger self-interactions $|\hat{\Lambda}| \sim 5.93 \times 10^{12}$ for the case $m_{22} \sim 1$ [105].[15] Astrophysical considerations can lead to further novel constraints; e.g., the soliton with the maximum mass and smallest radius is matched to the smallest galaxy then known—Willman I—in Ref. [106]. By demanding that the halo of Willman I is dominated by the self-interacting soliton close to its maximum possible mass, the SFDM parameters were constrained to be $m_{22} = 193$ and $|\hat{\Lambda}| = 3.25 \times 10^8$. In that case, the critical mass for collapse of a soliton should be close to the Willman I mass, i.e., $M_{c,7}^{\max} \sim 0.1$, which is in agreement with one of our requirements of our ideal model (namely the one that requires collapse once the mass of the central soliton exceeds $M_{c,7}^{\max} = 0.1$–10). However, this estimate does not fulfill the other condition of obtaining collapse once $M_{h,12}^{(\text{crit})} = 10^{-2} - 1$.

Another interesting result is presented in Ref. [107], where the addition of the attractive self-interaction, in terms of the full trigonometric axion potential, is taken into

---

[14]The self-interaction parameter is obtained as $\lambda = m^2/f^2$, where $f$ is the axion-decay constant. For an ultralight axion, the decay constant is of order $f \sim 10^{16}$ GeV.

[15]Notice that in terms of the parameter $\lambda$, these values for the self-interaction are extremely small, which corroborate the fact that self-interaction is usually ignored.

account. In this case, the bounds from the Lyman-$\alpha$ power spectrum on the particle mass $m$ are less restrictive than for free SFDM mentioned above.

Now, in this subsection, we shall proceed in the same way as for the previous SFDM models; i.e., we shall try to find the region of parameters where our ideal model of SMBH formation can be fulfilled. The first thing we can see is that, different from the previous cases, once we compare the critical mass $M_{h,12}^{(\text{crit})}$ (81) or (89) and the maximum possible mass for the soliton $M_{c,7}^{\max}$ (82), the way each quantity depends on the free parameters of SFDM is different. It is this difference that can help us to fulfill our ideal model more easily. Let us first consider the extension that is based upon the results of Schive *et al.* [19,31]. In fact, using (81) and (82), our ideal model works out, as long as the SFDM parameters fulfil

$$|\hat{\Lambda}| = 4.29 \times 10^6 - 9.24 \times 10^7, \qquad (102\text{a})$$

$$m_{22}|\hat{\Lambda}|^{1/2} = 2.05 \times 10^4 - 2.05 \times 10^6. \qquad (102\text{b})$$

This region of parameters is shown in Fig. 6 (they are marked in green in the upper and lower figures). We can combine these two last expressions to obtain an estimate for the mass parameter. For example, if we adopt the value $|\hat{\Lambda}| = 4.29 \times 10^6$ (i.e., if we demand to obtain collapse once $M_{h,12}^{(\text{crit})} = 1$), the particle mass should be in the range $m_{22} = 9.90 - 9.90 \times 10^2$ in order to fit our fiducial choice of $M_{c,7}^{\max} = 0.1$–$10$. If, on the other hand, we adopt $|\hat{\Lambda}| = 9.24 \times 10^7$ (we demand to obtain collapse once $M_{h,12}^{(\text{crit})} = 10^{-2}$), we obtain $m_{22} = 2.14 - 2.14 \times 10^2$. Then, we can roughly estimate that the favored mass for SMBH formation should be in the range

$$m_{22} \simeq 2.14 - 9.90 \times 10^2. \qquad (102\text{c})$$

Now, we turn to the extension which is based upon the results of Mocz *et al.* [34], using (89) and (82). In this case, our ideal model works out, as long as the SFDM parameters satisfy

$$m_{22}|\hat{\Lambda}|^{3/2} = 7.56 \times 10^6 - 1.63 \times 10^{10}, \qquad (103\text{a})$$

$$m_{22}|\hat{\Lambda}|^{1/2} = 2.05 \times 10^4 - 2.05 \times 10^6. \qquad (103\text{b})$$

We have also shown this region of parameters in Fig. 6 (they are marked in green in the middle and bottom figures). If we proceed to do an analysis similar to the one we did to estimate (102c), we finally arrive at the preferable parameters for SMBH formation:

$$|\hat{\Lambda}| = 3.69 - 7.95 \times 10^5, \qquad (103\text{c})$$
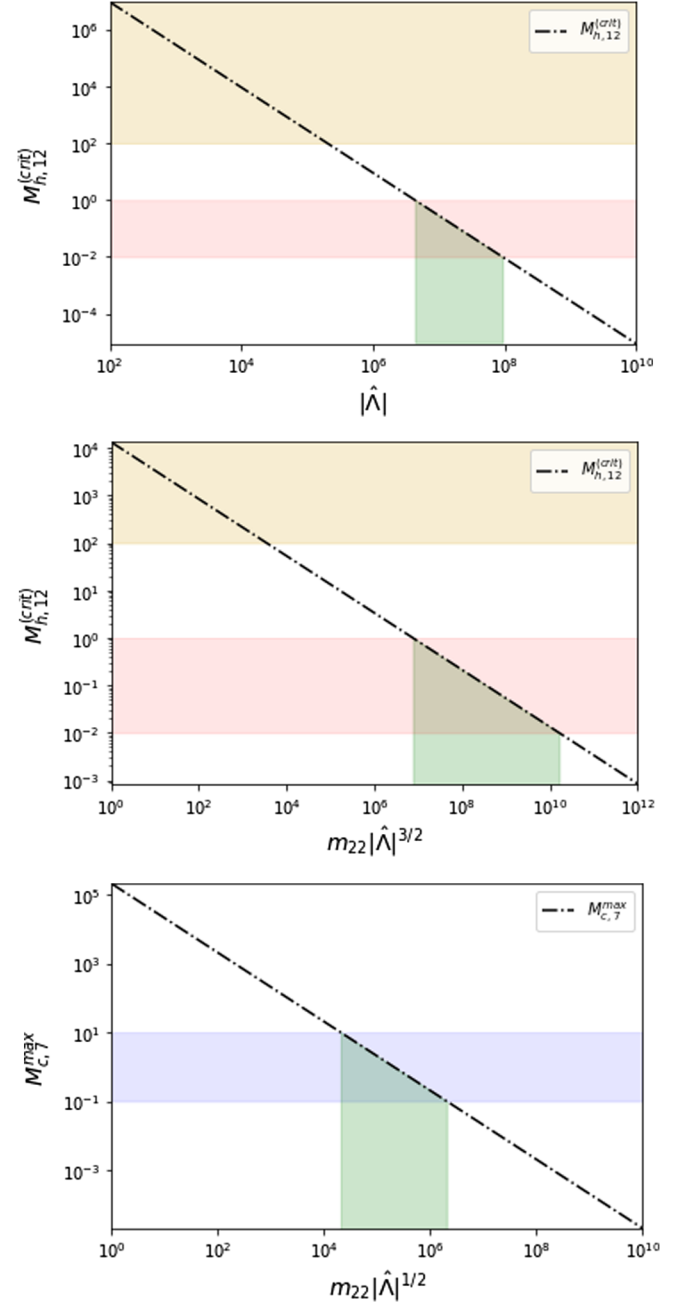


FIG. 6.　Top: $M_{h,12}^{(\text{crit})}$ as a function of $|\hat{\Lambda}|$ for our *Schive et al.* [19,31]. extension. Middle: $M_{h,12}^{(\text{crit})}$ as a function of $m_{22}|\hat{\Lambda}|^{3/2}$ for our *Mocz et al.* [34] extension. Bottom: $M_{c,7}^{\max}$ as a function of $m_{22}|\hat{\Lambda}|^{1/2}$. The blue, red, golden, and green regions indicate the same meaning as in Fig. 4.

$$m_{22} = 22.99 - 1.7 \times 10^4. \qquad (103\text{d})$$

Finally, we need to compare our estimates to previous constraints. This comparison is more difficult to do since, as we mentioned earlier, attractive SFDM has not been explored with much detail in this context. However, we can

see that our estimates of the self-interaction term seem to be quite close to those reported by other works.

Now, in addition, we can adopt our estimates as independent constraints with respect to the possible formation of SMBHs. The parameter region $|\hat{\Lambda}| > 9.24 \times 10^7$ for our Schive *et al.* [19,31] extension or $m_{22}|\hat{\Lambda}|^{3/2} > 1.63 \times 10^{10}$ for our Mocz *et al.* [34] extension would be ruled out, if we want to avoid formation of SMBHs for the lightest galactic halos (e.g., those hosting small dSphs). The same happens for the range of parameters $|\hat{\Lambda}| = 1.99 \times 10^5 - 4.29 \times 10^6$ and $m_{22}|\hat{\Lambda}|^{3/2} = 3.51 \times 10^3 - 7.56 \times 10^6$, which is ruled out in order to avoid collapse in galactic halos which are too massive. Finally, demanding non-formation of SMBHs imposes the constraint $|\hat{\Lambda}| \leq 1.99 \times 10^5$, using our Schive *et al.* [19,31] extension, and $m_{22}|\hat{\Lambda}|^{3/2} \leq 3.51 \times 10^3$, using our Mocz *et al.* [34] extension, which is a region of parameters that fits previous constraints.

## VI. CONCLUSIONS

We have studied the SFDM core-halo mass relations, which have been reported in various previous simulation papers. Our main objective was the extension of these relations for SFDM models which include self-interaction. After presenting the basic equations used to model SFDM, we adopted a Gaussian ansatz to describe typical core/soliton structures of this model. We showed that this ansatz can correctly reproduce several properties of the numerical results that are well known for these solitons, with a special emphasis on the question beyond which critical mass those solitons will collapse. This question is of immediate importance, once we realize that the core-halo mass relations imply that such soliton collapse could happen, once the mass of the halo itself exceeds a certain threshold. This has implications for SFDM with or without self-interaction. We showed how the core-halo mass relation, typically found in numerical simulations of structure formation in the free SFDM model, can be generalized to models with self-interaction. Basically, two different core-halo mass relations have been reported in the literature for free SFDM; hence, we decided to extend both of them. Using our extendend core-halo mass relations, we constrain the free parameters of the SFDM model by exploring the possibility of SMBH formation in massive galactic halos. Comparing our findings with previous constraints reported by other groups through different observational evidence—not related to the SMBH formation considered here—we show that soliton collapse to form SMBHs is favored neither in SFDM models without self-interaction nor in those with repulsive self-interaction. In these cases, the central solitons will never get close to the critical mass of collapse. However, if, on the other hand, we accept a range of parameters that are beyond those commonly reported for these two scenarios, i.e., if we adopted a much smaller de

Broglie wavelength for the free-field SFDM model or a much smaller ($n = 1$)-polytrope radius for the repulsive scenario, it turns out that it is possible to explain the formation of SMBHs with masses in the desired range for one of the two core-halo mass relations we explored. However, in adopting such a range, SFDM becomes indistinguishable from CDM during structure formation, since the scale of suppressing small-scale structure is greatly reduced for that range of parameters. However, this does not mean that such a model of SFDM is not a viable one for cosmic DM, since it would be hard to distinguish it from CDM (except perhaps by direct detection or annihilation effects of the latter), and that additionally it would have a natural mechanism to explain the formation of SMBHs. To conclude with our study, we found that in SFDM with attractive self-interaction, SMBH formation is feasible more easily since it is possible to fulfil our ideal model of SMBH formation completely and for both core-halo mass extensions. Only few studies have been done that constrain the free parameters of attractive SFDM (by not ignoring the contribution of the self-interaction term), so our results, that we obtained for this case, serve as additional, independent constraints for the model.

More simulation work will be required in order to settle the question of which core-halo mass relation should be expected in SFDM models with and without self-interaction. In this work, we have built upon the existing literature, which presents us with two different exponents for the core-halo mass relation in free SFDM models. We have taken them at face value, performing analytic calculations in order to show for each case which modified relations are expected, once self-interaction is included. This way, our work makes clean predictions, which can be compared to upcoming simulations of SFDM structure formation.

## APPENDIX: ANALYTIC APPROXIMATIONS: GAUSSIAN VS SCHIVE PROFILE

Previous literature has made extensive use of two different analytic approximations for the central soliton in SFDM halos without self-interaction (the free case). On the one hand, there is a density distribution $\rho_c^{(p)}$ given by Ref. [19] (Schive profile),

$$\rho_c^{(p)}(r) = \frac{\rho_0}{(1 + 0.091(\frac{r}{r_c})^2)^8}, \qquad (A1)$$

where $\rho_0$ is the central density of the soliton

$$\rho_0 = 1.93 \times 10^7 m_{22}^{-2} \left(\frac{r_c}{1 \text{ kpc}}\right)^{-4} M_\odot \text{kpc}^{-3} \qquad (A2)$$

and the core radius $r_c$ is defined as the radius where the mass density drops by a factor of 2 from its value at the origin,

$$r_c \simeq \frac{2.27 \times 10^4}{(m_{22})^2 M_{c,7}} pc. \qquad (A3)$$

On the other hand, it has been noted that the soliton profile can be also well approximated by a Gaussian density distribution $\rho_c^{(g)}$ [38],

$$\rho_c^{(g)}(r) = \frac{M_c}{(\pi R_c^2)^{3/2}} e^{-r^2/R_c^2}, \qquad (A4)$$

where we take $R_c$ in such a way that the radius that contains 99% of the mass of the Gaussian ansatz matches with the numerical solution. Then,

$$R_c \simeq \frac{3.54 \times 10^4}{(m_{22})^2 M_{c,7}} pc. \qquad (A5)$$

Observe from (17) that both cases, Eqs. (A1) and (A4), follow the same rescaling dependence $\rho_c^{(p)}, \rho_c^{(g)} \propto \gamma^{-4}$, as expected.

We can compare the above analytic profiles with the numerical solution. For that purpose, it is convenient to rewrite each approximation in terms of dimensionless variables (15), i.e., "hat" quantities, and by considering the solution that has a central scalar field value equal to 1. In this manner, we can compare each approximation with the numerical solution with $\gamma = 1$. We note that the analytic approach given in (A1) results in a better approximation for the soliton at small $\hat{r}$ than the Gaussian, as can be seen from Fig. 7. In the top figure, we plot the dimensionless squared wave function $|\hat{\psi}^{(1)}|^2$, where
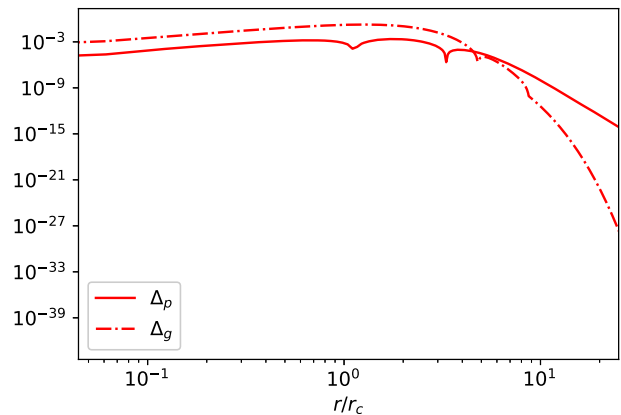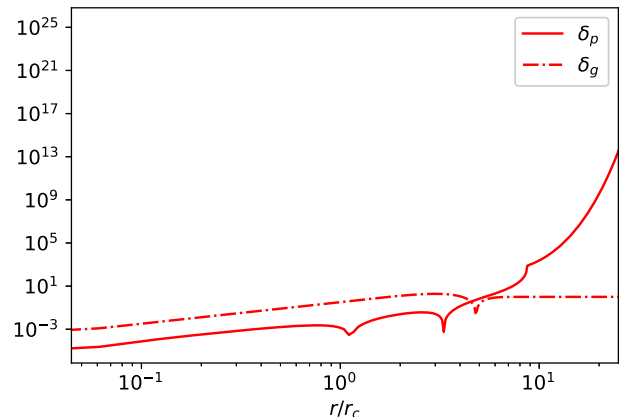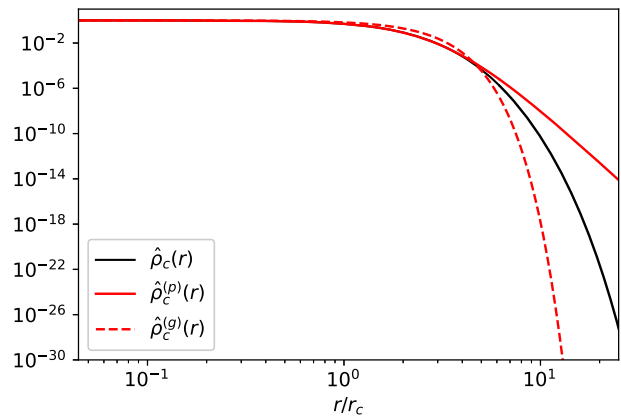


FIG. 7. Schive profile (red solid) vs Gaussian (red dashed) density distributions. In the top figure, we plot each case and the numerical solution (black solid), while in the bottom figures, we plot the relative (middle) and the absolute (bottom) errors for each approximation.

superscript 1 refers to $\gamma = 1$, together with the Gaussian and the Schive profile. The middle figure shows the relative error $\delta_i \equiv |(\hat{\rho}_c^{(1)} - \hat{\rho}_c^{(i)})/\hat{\rho}_c^{(i)}|$, $i = p, g$, while the bottom figure shows the total error $\Delta_i \equiv |\hat{\rho}_c^{(1)} - \hat{\rho}_c^{(i)}|$, $i = p, g$ for each approximation.

[1] P. J. E. Peebles, Large-scale background temperature and mass fluctuations due to scale-invariant primeval perturbations, Astrophys. J. **263**, L1 (1982).

[2] S. D. White, C. S. Frenk, M. Davis, and G. Efstathiou, Clusters, filaments, and voids in a universe dominated by cold dark matter, Astrophys. J. **313**, 505 (1987).

[3] J. S. Bullock and M. Boylan-Kolchin, Small-scale challenges to the Λcdm paradigm, Annu. Rev. Astron. Astrophys. **55**, 343 (2017).

[4] D. Clowe, M. Bradač, A. H. González, M. Markevitch, S. W. Randall, C. Jones, and D. Zaritsky, A direct empirical proof of the existence of dark matter, Astrophys. J. Lett. **648**, L109 (2006).

[5] A. Klypin, A. V. Kravtsov, O. Valenzuela, and F. Prada, Where are the missing galactic satellites?, Astrophys. J. **522**, 82 (1999).

[6] B. Moore, S. Ghigna, F. Governato, and G. Lake, G. T. Quinn, J. Stadel, and P. Tozzi, Dark matter substructure within galactic halos, Astrophys. Lett. **524**, L19 (1999).

[7] S. J. Penny, C. J. Conselice, S. De Rijcke, and E. V. Held, Hubble space telescope survey of the perseus cluster–i. The structure and dark matter content of cluster dwarf spheroidals, Mon. Not. R. Astron. Soc. **393**, 1054 (2009).

[8] J. M. Gaskins, A review of indirect searches for particle dark matter, Contemp. Phys. **57**, 496 (2016).

[9] A. Arbey, J. Lesgourgues, and P. Salati, Cosmological constraints on quintessential halos, Phys. Rev. D **65**, 083514 (2002).

[10] V. Sahni and L. Wang, New cosmological model of quintessence and dark matter, Phys. Rev. D **62**, 103517 (2000).

[11] W. Hu, R. Barkana, and A. Gruzinov, Fuzzy Cold Dark Matter: The Wave Properties of Ultralight Particles, Phys. Rev. Lett. **85**, 1158 (2000).

[12] T. Matos and L. A. Ureña López, Further analysis of a cosmological model with quintessence and scalar dark matter, Phys. Rev. D **63**, 063506 (2001).

[13] T. Matos and L. A. Ureña López, Quintessence and scalar dark matter in the universe, Classical Quantum Gravity **17**, L75 (2000).

[14] T. Matos, F. S. Guzmán, and L. A. Ureña López, Scalar field as dark matter in the universe, Classical Quantum Gravity **17**, 1707 (2000).

[15] A. Arbey, J. Lesgourgues, and P. Salati, Quintessential halos around galaxies, Phys. Rev. D **64**, 123528 (2001).

[16] A. Arbey, J. Lesgourgues, and P. Salati, Galactic halos of fluid dark matter, Phys. Rev. D **68**, 023511 (2003).

[17] S.-J. Sin, Late-time phase transition and the galactic halo as a Bose liquid, Phys. Rev. D **50**, 3650 (1994).

[18] S. Ji and S.-J. Sin, Late-time phase transition and the galactic halo as a Bose liquid. ii. the effect of visible matter, Phys. Rev. D **50**, 3655 (1994).

[19] H.-Y. Schive, T. Chiueh, and T. Broadhurst, Cosmic structure as the quantum interference of a coherent dark wave, Nat. Phys. **10**, 496 (2014).

[20] C. Boehmer and T. Harko, Can dark matter be a Bose-Einstein condensate?, J. Cosmol. Astropart. Phys. 07 (2007) 025.

[21] D. J. Marsh and P. G. Ferreira, Ultralight scalar fields and the growth of structure in the universe, Phys. Rev. D **82**, 103528 (2010).

[22] M. Membrado, A. Pacheco, and J. Sañudo, Hartree solutions for the self-Yukawian boson sphere, Phys. Rev. A **39**, 4207 (1989).

[23] F. S. Guzmán, T. Matos, and H. Villegas, Scalar fields as dark matter in spiral galaxies: Comparison with experiments, Astron. Nachr. **320**, 97 (1999).

[24] F. S. Guzmán and T. Matos, Scalar fields as dark matter in spiral galaxies, Classical Quantum Gravity **17**, L9 (2000).

[25] J. Magaña and T. Matos, A brief review of the scalar field dark matter model, J. Phys. Conf. Ser. **378**, 012012 (2012).

[26] A. Suárez, V. H. Robles, and T. Matos, A review on the scalar field/Bose-Einstein condensate dark matter model, in *Accelerated Cosmic Expansion* (Springer, New York, 2014), pp. 107–142.

[27] D. J. Marsh, Axion cosmology, Phys. Rep. **643**, 1 (2016).

[28] L. Hui, J. P. Ostriker, S. Tremaine, and E. Witten, Ultralight scalars as cosmological dark matter, Phys. Rev. D **95**, 043541 (2017).

[29] J. C. Niemeyer, Small-scale structure of fuzzy and axion-like dark matter, arXiv:1912.07064.

[30] T. Rindler-Daller and P. R. Shapiro, Complex scalar field dark matter on galactic scales, Mod. Phys. Lett. A **29**, 1430002 (2014).

[31] H.-Y. Schive, M.-H. Liao, T.-P. Woo, S.-K. Wong, T. Chiueh, T. Broadhurst, and W. P. Hwang, Understanding the Core-Halo Relation of Quantum Wave Dark Matter from 3d Simulations, Phys. Rev. Lett. **113**, 261302 (2014).

[32] B. Schwabe, J. C. Niemeyer, and J. F. Engels, Simulations of solitonic core mergers in ultralight axion dark matter cosmologies, Phys. Rev. D **94**, 043513 (2016).

[33] J. Veltmaat and J. C. Niemeyer, Cosmological particle-in-cell simulations with ultralight axion dark matter, Phys. Rev. D **94**, 123523 (2016).

[34] P. Mocz, M. Vogelsberger, V. H. Robles, J. Zavala, M. Boylan-Kolchin, A. Fialkov, and L. Hernquist, Galaxy formation with BECDM-I. Turbulence and relaxation of idealized haloes, Mon. Not. R. Astron. Soc. **471**, 4559 (2017).

[35] D. Levkov, A. Panin, and I. Tkachev, Gravitational Bose-Einstein Condensation in the Kinetic Regime, Phys. Rev. Lett. **121**, 151301 (2018).

[36] M. Mina, D. F. Mota, and H. A. Winther, Solitons in the dark: Non-linear structure formation with fuzzy dark matter, arXiv:2007.04119.

[37] M. Nori and M. Baldi, Scaling relations of fuzzy dark matter haloes i: Individual systems in their cosmological environment, arXiv:2007.01316.

[38] P.-H. Chavanis, Mass-radius relation of Newtonian self-gravitating Bose-Einstein condensates with short-range interactions. i. analytical results, Phys. Rev. D **84**, 043531 (2011).

[39] D. J. Marsh and A.-R. Pop, Axion dark matter, solitons and the Cusp–Core problem, Mon. Not. R. Astron. Soc. **451**, 2479 (2015).

[40] S.-R. Chen, H.-Y. Schive, and T. Chiueh, Jeans analysis for dwarf spheroidal galaxies in wave dark matter, Mon. Not. R. Astron. Soc. **468**, 1338 (2017).

[41] M. Cappellari, Astrophysics: Monster black holes, Nature (London) **480,** 187 (2011).

[42] N. J. McConnell, C.-P. Ma, K. Gebhardt, S. A. Wright, J. D. Murphy, T. R. Lauer, J. R. Graham, and D. O. Richstone, Two ten-billion-solar-mass black holes at the centres of giant elliptical galaxies, Nature (London) **480,** 215 (2011).

[43] Y. Matsuoka, M. Onoue, N. Kashikawa, M. A. Strauss, K. Iwasawa, C.-H. Lee, M. Imanishi, T. Nagao, M. Akiyama, N. Asami et al., Discovery of the first low-luminosity quasar at z> 7, Astrophys. J. Lett. **872,** L2 (2019).

[44] Y. Matsuoka, M. A. Strauss, N. Kashikawa, M. Onoue, K. Iwasawa, J.-J. Tang, C.-H. Lee, M. Imanishi, T. Nagao, M. Akiyama et al., Subaru high-z exploration of low-luminosity quasars (shellqs). v. quasar luminosity function and contribution to cosmic reionization at z = 6, Astrophys. J. **869,** 150 (2018).

[45] Y. Matsuoka, K. Iwasawa, M. Onoue, N. Kashikawa, M. A. Strauss, C.-H. Lee, M. Imanishi, T. Nagao, M. Akiyama, N. Asami et al., Subaru high-z exploration of low-luminosity quasars (shellqs). iv. discovery of 41 quasars and luminous galaxies at $5.7 \leq z \leq 6.9$, Astrophys. J. Suppl. Ser. **237,** 5 (2018).

[46] Y. Matsuoka, M. Onoue, N. Kashikawa, K. Iwasawa, M. A. Strauss, T. Nagao, M. Imanishi, C.-H. Lee, M. Akiyama, N. Asami et al., Subaru high-z exploration of low-luminosity quasars (shellqs). ii. Discovery of 32 quasars and luminous galaxies at $5.7 < z \leq 6.8$, Publ. Astron. Soc. Jpn. **70,** S35 (2017).

[47] Y. Matsuoka, M. Onoue, N. Kashikawa, K. Iwasawa, M. A. Strauss, T. Nagao, M. Imanishi, M. Niida, Y. Toba, M. Akiyama et al., Subaru high-z exploration of low-luminosity quasars (shellqs). i. discovery of 15 quasars and bright galaxies at $5.7 < z < 6.9$, Astrophys. J. **828,** 26 (2016).

[48] X.-B. Wu, F. Wang, X. Fan, W. Yi, W. Zuo, F. Bian, L. Jiang, I. D. McGreer, R. Wang, J. Yang et al., An ultraluminous quasar with a twelve-billion-solar-mass black hole at redshift 6.30, Nature (London) **518,** 512 (2015).

[49] X. Fan, M. A. Strauss, D. P. Schneider, R. H. Becker, R. L. White, Z. Haiman, M. Gregg, L. Pentericci, E. K. Grebel, V. K. Narayanan et al., A survey of $z > 5.7$ quasars in the sloan digital sky survey. ii. discovery of three additional quasars at $z > 6$, Astron. J. **125,** 1649 (2003).

[50] L. Jiang, X. Fan, M. Vestergaard, J. D. Kurk, F. Walter, B. C. Kelly, and M. A. Strauss, Gemini near-infrared spectroscopy of luminous $z \sim 6$ quasars: Chemical abundances, black hole masses, and Mg II absorption, Astron. J. **134,** 1150 (2007).

[51] C. J. Willott, P. Delorme, A. Omont, J. Bergeron, X. Delfosse, T. Forveille, L. Albert, C. Reylé, G. J. Hill, M. Gully-Santiago et al., Four quasars above redshift 6 discovered by the Canada-France high-z quasar survey, Astron. J. **134,** 2435 (2007).

[52] L. Jiang, X. Fan, J. Annis, R. H. Becker, R. L. White, K. Chiu, H. Lin, R. H. Lupton, G. T. Richards, M. A. Strauss et al., A survey of $z \sim 6$ quasars in the sloan digital sky survey deep stripe. I. a flux-limited sample at $z_{SB} < 21$, Astron. J. **135,** 1057 (2008).

[53] C. J. Willott, P. Delorme, C. Reylé, L. Albert, J. Bergeron, D. Crampton, X. Delfosse, T. Forveille, J. B. Hutchings, R. J. McLure et al., The Canada-France high-z quasar survey: Nine new quasars and the luminosity function at redshift 6, Astron. J. **139,** 906 (2010).

[54] D. J. Mortlock, S. J. Warren, B. P. Venemans, M. Patel, P. C. Hewett, R. G. McMahon, C. Simpson, T. Theuns, E. A. Gonzáles-Solares, A. Adamson et al., A luminous quasar at a redshift of $z = 7.085$, Nature (London) **474,** 616 (2011).

[55] B. Venemans, J. Findlay, W. Sutherland, G. De Rosa, R. McMahon, R. Simcoe, E. González-Solares, K. Kuijken, and J. Lewis, Discovery of three $z > 6.5$ quasars in the vista kilo-degree infrared galaxy (viking) survey, Astrophys. J. **779,** 24 (2013).

[56] E. Bañados, B. Venemans, E. Morganson, R. Decarli, F. Walter, K. Chambers, H.-W. Rix, E. Farina, X. Fan, L. Jiang et al., Discovery of eight $z \sim 6$ quasars from Pan-STARRS1, Astron. J. **148,** 14 (2014).

[57] J. Silk and M. J. Rees, Quasars and galaxy formation, arXiv:astro-ph/9801013.

[58] K. Freese, C. Ilie, D. Spolyar, M. Valluri, and P. Bodenheimer, Supermassive dark stars: Detectable in JWST, Astrophys. J. **716,** 1397 (2010).

[59] T. Rindler-Daller, M. H. Montgomery, K. Freese, D. E. Winget, and B. Paxton, Dark stars: Improved models and first pulsation results, Astrophys. J. **799,** 210 (2015).

[60] K. Menou, Z. Haiman, and V. K. Narayanan, The merger history of supermassive black holes in galaxies, Astrophys. J. **558,** 535 (2001).

[61] D. Merritt and L. Ferrarese, The $M$-$\sigma$ relation for supermassive black holes, Astrophys. J. **547,** 140 (2001).

[62] K. Gebhardt, R. Bender, G. Bower, A. Dressler, S. Faber, A. V. Filippenko, R. Green, C. Grillmair, L. C. Ho, J. Kormendy et al., A relationship between nuclear black hole mass and galaxy velocity dispersion, Astrophys. J. Lett. **539,** L13 (2000).

[63] L. Ferrarese, Beyond the bulge: A fundamental relation between supermassive black holes and dark matter halos, Astrophys. J. **578,** 90 (2002).

[64] K. Bandara, D. Crampton, and L. Simard, A relationship between supermassive black hole mass and the total gravitational mass of the host galaxy, Astrophys. J. **704,** 1135 (2009).

[65] A. Ávilez, T. Bernal, L. E. Padilla, and T. Matos, On the possibility that ultra-light boson haloes host and form supermassive black holes, Mon. Not. R. Astron. Soc. **477,** 3257 (2018).

[66] E. Seidel and W.-M. Suen, Dynamical evolution of boson stars: Perturbing the ground state, Phys. Rev. D **42,** 384 (1990).

[67] E. Seidel and W.-M. Suen, Oscillating Soliton Stars, Phys. Rev. Lett. **66,** 1659 (1991).

[68] E. Seidel and W.-M. Suen, Formation of Solitonic Stars Through Gravitational Cooling, Phys. Rev. Lett. **72,** 2516 (1994).

[69] N. Sanchis-Gual, J. C. Degollado, J. A. Font, C. Herdeiro, and E. Radu, Dynamical formation of a hairy black hole in a cavity from the decay of unstable solitons, Classical Quantum Gravity **34,** 165001 (2017).

[70] M. Alcubierre, F. S. Guzmán, T. Matos, D. Nuñez, L. A. Ureña López, and P. Wiederhold, Galactic collapse of scalar field dark matter, Classical Quantum Gravity **19,** 5017 (2002).

[71] J. Barranco, A. Bernal, J. C. Degollado, A. Diez-Tejedor, M. Megevand, M. Alcubierre, D. Núñez, and O. Sarbach, Are black holes a serious threat to scalar field dark matter models?, Phys. Rev. D **84,** 083008 (2011).

[72] J. Barranco, A. Bernal, J. C. Degollado, A. Diez-Tejedor, M. Megevand, M. Alcubierre, D. Núñez, and O. Sarbach, Schwarzschild Black Holes can Wear Scalar Wigs, Phys. Rev. Lett. **109,** 081102 (2012).

[73] R. Ruffini and S. Bonazzola, Systems of self-gravitating particles in general relativity and the concept of an equation of state, Phys. Rev. **187,** 1767 (1969).

[74] F. S. Guzmán and L. A. Urena-López, Evolution of the Schrödinger-Newton system for a self-gravitating scalar field, Phys. Rev. D **69,** 124033 (2004).

[75] F. S. Guzmán and L. A. Ureña López, Gravitational cooling of self-gravitating Bose condensates, Astrophys. J. **645,** 814 (2006).

[76] N. Bar, D. Blas, K. Blum, and S. Sibiryakov, Galactic rotation curves versus ultralight dark matter: Implications of the soliton-host Halo relation, Phys. Rev. D **98,** 083027 (2018).

[77] N. Bar, K. Blum, R. Sato, and J. Eby, Ultra-light dark matter in disk galaxies, Phys. Rev. D **99,** 103020 (2019).

[78] P.-H. Chavanis and L. Delfini, Mass-radius relation of Newtonian self-gravitating Bose-Einstein condensates with short-range interactions. ii. numerical results, Phys. Rev. D **84,** 043532 (2011).

[79] J. Eby, C. Kouvaris, N. G. Nielsen, and L. Wijewardhana, Boson stars from self-interacting dark matter, J. High Energy Phys. 02 (2016) 028.

[80] F. Guzmán and A. A. Ávilez, Head-on collision of multistate ultralight BEC dark matter configurations, Phys. Rev. D **97,** 116003 (2018).

[81] G. Baym and C. J. Pethick, Ground-State Properties of Magnetically Trapped Bose-Condensed Rubidium Gas, Phys. Rev. Lett. **76,** 6 (1996).

[82] J. Goodman, Repulsive dark matter, New Astron. **5,** 103 (2000).

[83] P. Peebles, Fluid dark matter, Astrophys. J. Lett. **534,** L127 (2000).

[84] S. L. Liebling and C. Palenzuela, Dynamical boson stars, Living Rev. Relativity **20,** 5 (2017).

[85] M. Colpi, S. L. Shapiro, and I. Wasserman, Boson stars: Gravitational equilibria of self-interacting scalar fields, Phys. Rev. Lett. **57,** 2485 (1986).

[86] P.-H. Chavanis, Core mass–halo mass relation of bosonic and fermionic dark matter halos harbouring a supermassive black hole, arXiv:1911.01937.

[87] P.-H. Chavanis, Predictive model of BEC dark matter halos with a solitonic core and an isothermal atmosphere, Phys. Rev. D **100,** 083022 (2019).

[88] P.-H. Chavanis, Derivation of a generalized Schrödinger equation for dark matter halos from the theory of scale relativity, Phys. Dark Universe **22,** 80 (2018).

[89] C. P. Ahn, A. C. Seth, M. Den Brok, J. Strader, H. Baumgardt, R. Van Den Bosch, I. Chilingarian, M. Frank, M. Hilker, R. McDermid *et al.*, Detection of supermassive black holes in two virgo ultracompact dwarf galaxies, Astrophys. J. **839,** 72 (2017).

[90] A. E. Reines, J. J. Condon, J. Darling, and J. E. Greene, A new sample of (wandering) massive black holes in dwarf galaxies from high-resolution radio observations, Astrophys. J. **888,** 36 (2020).

[91] R. Abbott, T. Abbott, S. Abraham, F. Acernese, K. Ackley, C. Adams, R. Adhikari, V. Adya, C. Affeldt, M. Agathos *et al.*, Gw190521: A Binary Black Hole Merger with a Total Mass of 150 $M_\odot$, Phys. Rev. Lett. **125,** 101102 (2020).

[92] A. Paredes and H. Michinel, Interference of dark matter solitons and galactic offsets, Phys. Dark Universe **12,** 50 (2016).

[93] A. X. González-Morales, D. J. Marsh, J. Peñarrubia, and L. A. Ureña-López, Unbiased constraints on ultralight axion mass from dwarf spheroidal galaxies, Mon. Not. R. Astron. Soc. **472,** 1346 (2017).

[94] V. Lora, J. Magana, A. Bernal, F. Sánchez-Salcedo, and E. Grebel, On the mass of ultra-light bosonic dark matter from galactic dynamics, J. Cosmol. Astropart. Phys. 12 (2012) 011.

[95] E. Calabrese and D. N. Spergel, Ultra-light dark matter in ultra-faint dwarf galaxies, Mon. Not. R. Astron. Soc. **460,** 4397 (2016).

[96] A. Sarkar, R. Mondal, S. Das, S. K. Sethi, S. Bharadwaj, and D. J. Marsh, The effects of the small-scale DM power on the cosmological neutral hydrogen (HI) distribution at high redshifts, J. Cosmol. Astropart. Phys. 04 (2016) 012.

[97] E. Armengaud, N. Palanque-Delabrouille, C. Yèche, D. J. Marsh, and J. Baur, Constraining the mass of light bosonic dark matter using SDSS lyman-$\alpha$ forest, Mon. Not. R. Astron. Soc. **471,** 4606 (2017).

[98] V. Iršič, M. Viel, M. G. Haehnelt, J. S. Bolton, and G. D. Becker, First Constraints on Fuzzy Dark Matter from Lyman-$\alpha$ Forest Data and Hydrodynamical Simulations, Phys. Rev. Lett. **119,** 031302 (2017).

[99] B. Li, T. Rindler-Daller, and P. R. Shapiro, Cosmological constraints on Bose-Einstein-condensed scalar field dark matter, Phys. Rev. D **89,** 083536 (2014).

[100] A. Suárez and P.-H. Chavanis, Cosmological evolution of a complex scalar field with repulsive or attractive self-interaction, Phys. Rev. D **95,** 063515 (2017).

[101] L. E. Padilla, J. A. Vázquez, T. Matos, and G. Germán, Scalar field dark matter spectator during inflation: The effect of self-interaction, J. Cosmol. Astropart. Phys. 01 (2019) 056.

[102] B. Li, P. R. Shapiro, and T. Rindler-Daller, Bose-Einstein-condensed scalar field dark matter and the gravitational wave background from inflation: New cosmological constraints and its detectability by LIGO, Phys. Rev. D **96,** 063505 (2017).

[103] A. Suárez and P.-H. Chavanis, Hydrodynamic representation of the Klein-Gordon-Einstein equations in the weak field limit: General formalism and perturbations analysis, Phys. Rev. D **92,** 023510 (2015).

[104] L. Visinelli, Light axion-like dark matter must be present during inflation, Phys. Rev. D **96,** 023013 (2017).

[105] M. Cicoli, M. D. Goodsell, and A. Ringwald, The type IIB string axiverse and its low-energy phenomenology, J. High Energy Phys. 12 (2012) 146.

[106] P.-H. Chavanis, Collapse of a self-gravitating Bose-Einstein condensate with attractive self-interaction, Phys. Rev. D **94**, 083007 (2016).

[107] F. X. L. Cedeño, A. X. González-Morales, and L. A. Ureña-López, Ultralight DM bosons with an axion-like potential: Scale-dependent constraints revisited, arXiv: 2006.05037.

[108] http://www.iac.edu.mx/.